*International Geology Review*
Vol. 51, Nos. 9–11, September–November 2009, 777–823

# Cenozoic palaeocanyon evolution, Ancestral Cascades arc volcanism, and structure of the Hope Valley–Carson Pass region, Sierra Nevada, California

Jeanette C. Hagan[a]*, Cathy J. Busby[a], Keith Putirka[b] and Paul R. Renne[cd]

[a]*Department of Earth Science, University of California Santa Barbara, Santa Barbara, CA 93106, USA;* [b]*Department of Earth and Environmental Sciences, California State University, Fresno, CA 93710, USA;* [c]*Berkeley Geochronology Center, 2455 Ridge Rd, Berkeley, CA 94709, USA;* [d]*Department of Earth and Planetary Science, University of California, Berkeley, CA 94720, USA*

(*Accepted 20 April 2009*)

We use new geologic mapping, geochronological, and geochemical data on Tertiary volcanic, volcaniclastic, and intrusive rocks to investigate the volcanic, stratigraphic, and structural evolution of the Carson Pass region south of Lake Tahoe in the central Sierra Nevada. Volcanic and volcaniclastic rocks were deposited in east–west-trending palaeocanyons carved into Mesozoic granitic and metamorphic basement rocks; sediments were transported westwards towards the present-day Central Valley of California. In the Carson Pass–Hope Valley area, two palaeotributaries are preserved in faulted terrane east of the present-day Sierran crest (Hope Valley area); these merge at the crest to form one large, >7 km wide palaeocanyon that is undisrupted by faults west of the crest (Carson Pass–Kirkwood area). This single, large palaeocanyon roughly coincides with the present-day Mokelumne River drainage. New $^{40}Ar/^{39}Ar$ dates and stratigraphic data east of the crest, integrated with previously published data west of the crest, constrain the ages of strata and unconformities within the Hope Valley–Carson Pass–Kirkwood palaeocanyon system. We interpret three major erosional unconformities to record uplift events at ca. 23–16, 13.5–11, and 10–7 Ma. In other parts of the central Sierra, these uplift events are inferred to correspond to range-front faulting events. We propose the term 'Hope Valley Graben' for the structural feature mapped immediately east of the Sierran crest at Carson Pass. It is a nearly symmetrical full graben that offsets volcanic rocks as young as 6 Ma at least 400 m (1300 ft) on each of its bounding faults – herein named the Red Lake Fault on the west and the Hope Valley Fault on the east. However, we infer that faulting began before eruption of the 6 Ma volcanic rocks for three reasons: (1) the graben-localized emplacement of one of the largest volcanic centres in the Sierra, the 6.34 ± 0.14–6.18 ± 0.14 Ma Markleeville Peak Center; (2) andesite lava flows erupted at 6.22 ± 0.14 Ma from the Red Lake Fault, and abut it within the graben; and (3) brecciated granite along the Red Lake Fault is intruded by altered andesite, indicating that the fault started slipping before magmatism ceased. Our stratigraphic and geochronologic data do not permit an estimate of the amount of pre-6 Ma displacement in the Hope Valley graben. The geometry of the palaeocanyon system indicates that a dextral component of slip demonstrated for transtensional faults in other parts of the region did not operate in the Hope Valley graben.

**Keywords:** Sierra Nevada; Ancestral Cascades arc; Walker Lane Belt

*Corresponding author. Email: hagan@umail.ucsb.edu

ISSN 0020-6814 print/ISSN 1938-2839 online
© 2009 Taylor & Francis
DOI: 10.1080/00206810903028102
http://www.informaworld.com

## Introduction

In the central Sierra Nevada (Figure 1), Tertiary deposits of dominantly fragmental volcanic–volcaniclastic andesitic rocks of the Ancestral Cascades arc were deposited into, and are preserved in palaeochannels (Lindgren 1911; Curtis 1954; Wagner *et al.* 2000). Volcanic and volcaniclastic rocks from Carson Pass in the central Sierra Nevada record part of this palaeocanyon fill. These rocks record the late Cenozoic volcanotectonic history of the Sierra Nevada, including the deposition of Oligocene ignimbrites erupted in central Nevada, *in situ* Ancestral Cascades arc magmatism, initiation of Walker Lane transtensional faulting, and onset of Basin and Range extensional faulting.

In the Late Cretaceous, the Sierra Nevada formed the western edge of a Tibetan-type plateau, termed the 'Nevadaplano' (Coney and Harms 1984; Chase *et al.* 1998; Wolfe *et al.* 1998; DeCelles 2004), with a drainage divide in central Nevada (Henry 2008). Palaeorivers drained westwards across western Nevada and eastern California into the present-day Central Valley, carving wide canyons into the Sierra Nevada basement rock (Lindgren 1911; Bateman and Wahrhaftig 1966; Huber 1990; Wakabayashi and Sawyer 2001; Garside *et al.* 2005). During Oligocene time, large-volume caldera-forming eruptions in central Nevada produced ash flows that were funnelled down the channels across western Nevada and the Sierra Nevada (Davis *et al.* 2000; Henry *et al.* 2003). From the late Oligocene to early Miocene, the arc front swept westwards across Nevada, accompanying slab fallback (Wernicke 1992; Dilles and Gans 1995; Schweickert *et al.* 2004; Dickinson 2006; Cousens *et al.* 2008). Debris from calc-alkaline andesitic eruptions was transported westwards, down the palaeocanyons, as debris flows and streamflows. The calc-alkaline Ancestral Cascades arc swept westwards into the present-day northern and central Sierra Nevada by 16 Ma (Putirka and Busby 2007; Busby *et al.* 2008a,b; Cousens *et al.* 2008; Busby and Putirka 2009). New $^{40}Ar/^{39}Ar$ age data suggest that arc magmatism in the central Sierra occurred from ~16 to 6 Ma (Busby *et al.* 2008a,b; this paper).

A westward encroachment of normal faulting may have accompanied the westward magmatic sweep, although the timing and nature of onset of Sierran range-front faulting remains controversial (Dilles and Gans 1995; Trexler *et al.* 2000; Henry and Perkins 2001; Stockli *et al.* 2002; Surpless *et al.* 2002). Our recent research at Sonora Pass (Figure 1(a)) shows that dextral transtension began at that latitude by ~10 Ma, triggering high-K magmatism from the Little Walker Center (Putirka and Busby 2007; Busby *et al.* 2008b). We proposed that this centre formed at a releasing stepover of dextral transtensional faults at the inception of the Walker Lane Belt, and may record the birth of the future Pacific–North American plate boundary (Busby and Putirka 2009).

The Sierra Nevada lies within a microplate bounded to the west by the San Andreas Fault and to the east by the Walker Lane Belt (Figure 1), an ~150 km-wide zone of complex, dominantly northwest-striking, right-lateral strike-slip faults. GPS measurements reveal that the Walker Lane Belt currently accommodates ~20–25% of the Pacific–North America plate motion (Dixon *et al.* 1995; Thatcher *et al.* 1999; Dixon *et al.* 2000; Wernicke *et al.* 2000; Faulds *et al.* 2005). Field data from Sierra Nevada range-front faults are notably lacking, however, and thus very little is known of the long-term history of slip on them (Hearn and Humphreys 1998; Faulds *et al.* 2005).

Most existing maps of the central Sierra Nevada were made before modern volcanological facies analysis techniques were developed, and many Tertiary rocks of the region remain undivided. The Sierran Tertiary volcanic rocks are largely undated, making lithologic correlations tenuous at best, and relationships to structures unknown. Therefore, little is known about the volumes and compositions of magmas emplaced through time.

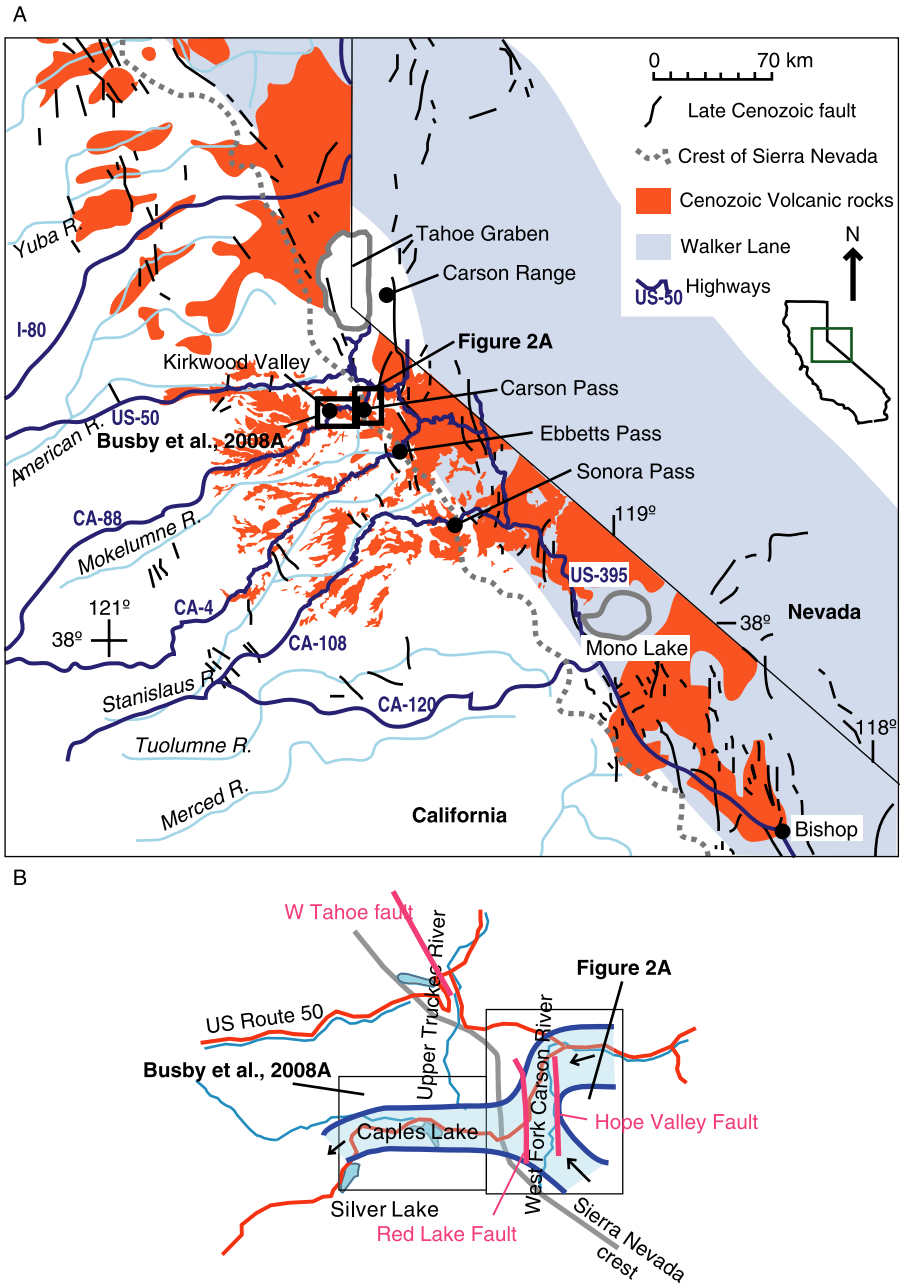


Figure 1. (a) Map of the central Sierra Nevada, showing modern drainages and the Sierra Nevada range crest, range-front faults (after Wakabayashi and Sawyer 2001), major roads, and distribution of Cenozoic volcanic–volcaniclastic rocks. Map area (Figure 2) and other localities of the central Sierra referred to in text are shown. (b) Inferred position of two palaeocanyon tributaries in the Hope Valley area that merge at the Sierran crest to form one palaeocanyon in the Carson Pass–Kirkwood area, based on mapping presented here (Figure 2(a)) and by Busby *et al.* (2008a). As discussed in the text, dextral transtensional motion is inferred from focal mechanisms and from geologic mapping of other range-front faults, but there is no evidence here for dextral offset of the palaeocanyon along range-front faults. Pink lines, faults; red lines, roads; arrows, palaeoflow direction.

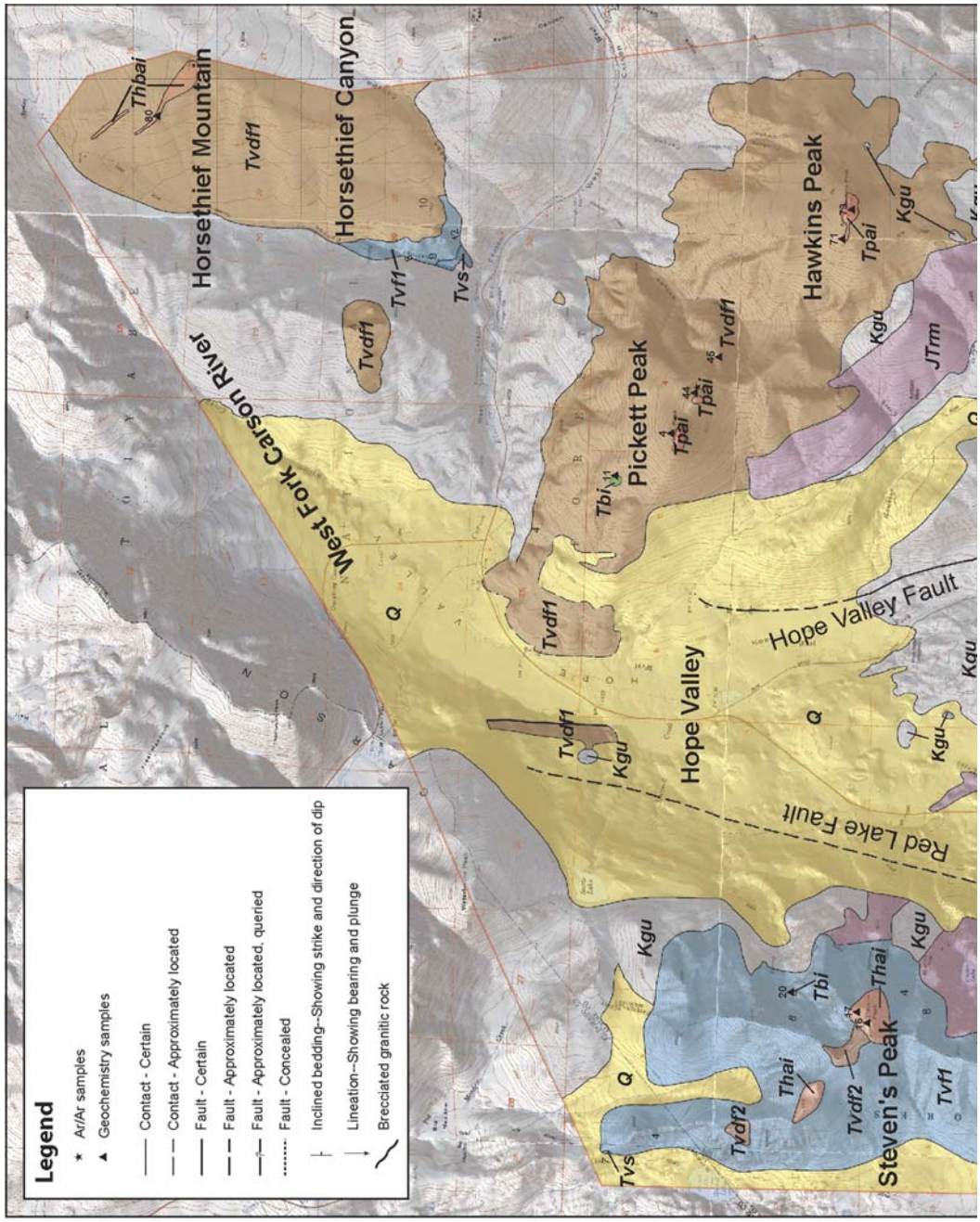
Legend
Ar/Ar samples
Geochemistry samples
Contact - Certain
Contact - Approximately located
Fault - Certain
Fault - Approximately located
Fault - Approximately located, queried
Fault - Concealed
Inclined bedding--Showing strike and direction of dip
Lineation--Showing bearing and plunge
Brecciated granitic rock
Horsethief Mountain
Horsethief Canyon
West Fork Carson River
Pickett Peak
Hawkins Peak
Hope Valley
Hope Valley Fault
Red Lake Fault
Steven's Peak
Thibai
Tvdf1
Tvf1
Tvs
Tbi
Tpai
Kgu
JTrm
Thai
Tvdf2
Q

(a)

Red Lake Peak
Elephant's Back
Red Lake
Charity Valley
Markleeville Peak
Jeff Davis Peak
Kgu
Q
Taa
JTrm
Tvf1
Tvf2
Tvdf1
Tvdf2
Thaba1
Thaba2
Thaba3
Thall
Thalu
Thbdi
Thadp
Tphaba
Tvs
Tsb
Tbai
Tbl
Tri
Tl
N
1,500 750 0 1,500 M

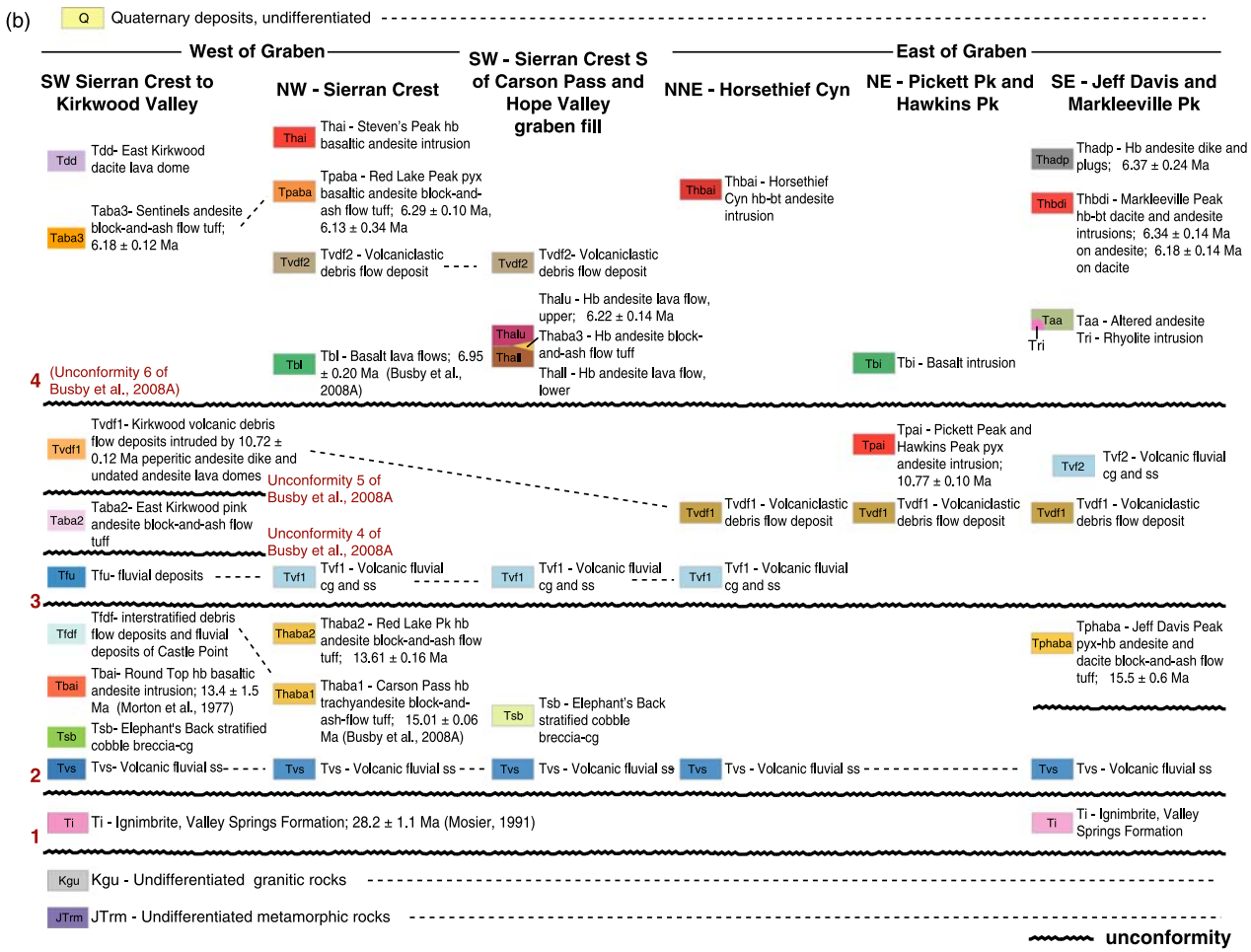
(b)
Q Quaternary deposits, undifferentiated
West of Graben
East of Graben
SW Sierran Crest to Kirkwood Valley
NW - Sierran Crest
SW - Sierran Crest S of Carson Pass and Hope Valley graben fill
NNE - Horsethief Cyn
NE - Pickett Pk and Hawkins Pk
SE - Jeff Davis and Markleeville Pk
Tdd Tdd- East Kirkwood dacite lava dome
Taba3 Taba3- Sentinels andesite block-and-ash flow tuff; 6.18 ± 0.12 Ma
Thai Thai - Steven's Peak hb basaltic andesite intrusion
Tpaba Tpaba - Red Lake Peak pyx basaltic andesite block-and-ash flow tuff; 6.29 ± 0.10 Ma, 6.13 ± 0.34 Ma
Tvdf2 Tvdf2 - Volcaniclastic debris flow deposit
Tvdf2 Tvdf2- Volcaniclastic debris flow deposit
Thbai Thbai - Horsethief Cyn hb-bt andesite intrusion
Thadp Thadp - Hb andesite dike and plugs; 6.37 ± 0.24 Ma
Thbdi Thbdi - Markleeville Peak hb-bt dacite and andesite intrusions; 6.34 ± 0.14 Ma on andesite; 6.18 ± 0.14 Ma on dacite
Thalu Thalu - Hb andesite lava flow, upper; 6.22 ± 0.14 Ma
Thaba3 Thaba3 - Hb andesite block-and-ash flow tuff
Thall Thall - Hb andesite lava flow, lower
Taa Taa - Altered andesite
Tri Tri - Rhyolite intrusion
Tbl Tbl - Basalt lava flows; 6.95 ± 0.20 Ma (Busby et al., 2008A)
Tbi Tbi - Basalt intrusion
4 (Unconformity 6 of Busby et al., 2008A)
Tvdf1 Tvdf1- Kirkwood volcanic debris flow deposits intruded by 10.72 ± 0.12 Ma peperitic andesite dike and undated andesite lava domes
Unconformity 5 of Busby et al., 2008A
Taba2 Taba2- East Kirkwood pink andesite block-and-ash flow tuff
Unconformity 4 of Busby et al., 2008A
Tpai Tpai - Pickett Peak and Hawkins Peak pyx andesite intrusion; 10.77 ± 0.10 Ma
Tvf2 Tvf2 - Volcanic fluvial cg and ss
Tvdf1 Tvdf1 - Volcaniclastic debris flow deposit
Tvdf1 Tvdf1 - Volcaniclastic debris flow deposit
Tvdf1 Tvdf1 - Volcaniclastic debris flow deposit
Tfu Tfu- fluvial deposits
Tvf1 Tvf1 - Volcanic fluvial cg and ss
Tvf1 Tvf1 - Volcanic fluvial cg and ss
Tvf1 Tvf1 - Volcanic fluvial cg and ss
3
Tfdf Tfdf- interstratified debris flow deposits and fluvial deposits of Castle Point
Tbai Tbai- Round Top hb basaltic andesite intrusion; 13.4 ± 1.5 Ma (Morton et al., 1977)
Tsb Tsb- Elephant's Back stratified cobble breccia-cg
Thaba2 Thaba2 - Red Lake Pk hb andesite block-and-ash flow tuff; 13.61 ± 0.16 Ma
Thaba1 Thaba1 - Carson Pass hb trachyandesite block-and-ash-flow tuff; 15.01 ± 0.06 Ma (Busby et al., 2008A)
Tsb Tsb - Elephant's Back stratified cobble breccia-cg
Tphaba Tphaba - Jeff Davis Peak pyx-hb andesite and dacite block-and-ash flow tuff; 15.5 ± 0.6 Ma
2
Tvs Tvs- Volcanic fluvial ss
Tvs Tvs - Volcanic fluvial ss
Tvs Tvs - Volcanic fluvial ss
Tvs Tvs - Volcanic fluvial ss
Tvs Tvs - Volcanic fluvial ss
1
Ti Ti - Ignimbrite, Valley Springs Formation; 28.2 ± 1.1 Ma (Mosier, 1991)
Ti Ti - Ignimbrite, Valley Springs Formation
Kgu Kgu - Undifferentiated granitic rocks
JTrm JTrm - Undifferentiated metamorphic rocks
unconformity

There are very few publications with detailed geologic maps that use modern volcanologic and stratigraphic approaches to report new geochemical and geochronological data (Busby *et al.* 2008a,b; Garrison *et al.* 2008; this paper).

The central Sierra Nevada is an ideal place to determine long-term slip history on Sierra range-front faults, because there are abundant Neogene volcanic–volcaniclastic and intrusive rocks that can be used to determine the nature and timing of range-front faulting relative to magmatic events (Busby *et al.* 2008b). The palaeocanyon fill also provides ideal piercing points with a trend roughly perpendicular to the faults.

In this paper, we describe the volcanic, volcaniclastic, and intrusive lithofacies that we use to divide the Cenozoic rocks into mappable units and use the map data to recognize unconformities within the section. We then interpret the palaeocanyon in a sequence stratigraphic framework, and propose a model to interpret the unconformities to record uplift events. Lastly, we present a model for the development of Sierra Nevada range-front faults at Carson Pass.

## Previous mapping

Unfaulted Tertiary rocks in the Carson Pass–Kirkwood area (Figure 1(a)), from the Sierran crest westwards, were undivided prior to the work of Busby *et al.* (2008a). That research showed that the 650 m deep Carson Pass–Kirkwood palaeocanyon preserves six unconformity-bounded sequences deposited between ~15 and 6 Ma (Busby *et al.* 2008a). We tentatively correlated the three deepest unconformities in the Carson Pass–Kirkwood palaeocanyon with unconformities of the same age in palaeocanyon fill of the Sonora Pass area about 50 km to the south (Figure 1). In both regions, these unconformities formed at ~16, ~11, and ~7 Ma (Busby *et al.* 2008b).

Tertiary rocks east of the crest, in the Hope Valley area (Figure 1), are faulted and less completely exposed than rocks of the Carson Pass–Kirkwood area. Previous mapping of two 15-min quadrangle maps covering the Hope Valley region (Armin *et al.* 1983, 1984) divided Tertiary rocks into undifferentiated volcanic–volcaniclastic rocks, which they referred to as Relief Peak Formation, as well as intrusions, which were further divided by mineralogy.

Figure 2. (a) Geologic map of the Hope Valley area; key to map units is given in (b). Mapping by Hagan in 2005 and 2008. Previous mapping by Armin *et al.* (1983, 1984) and Mosier (1991) described in text. Higher-resolution versions of this illustration are available via the 'Multimedia' tab on this article's page at www.informaworld.com (b) Chronostratigraphic correlation chart for the map units of the Kirkwood Valley–Carson Pass–Hope Valley area. These map units form the fill of, or intrude, the Hope Valley–Carson Pass–Kirkwood palaeocanyon system, shown in Figure 9. The column on the left edge displays the stratigraphy at Kirkwood Valley, taken from Figure 2 of Busby *et al.* (2008a). The NW Sierran crest column is updated from that map, based on more detailed geologic mapping and geochronology completed for this study. Map unit Thaba1 in this paper was labelled Taba1 in Busby *et al.* (2008a). The other four columns represent stratigraphic relationships recognized in the present study (Figure 2(a)). Unconformity surfaces are noted by zigzag bold black lines and labelled at left in red. Unconformity 1 records Late Cretaceous unroofing of the Sierra Nevada batholith during low-angle subduction (Busby and Putirka 2009). Unconformities 2–4 can be traced along the mapped length of the palaeocanyon system, from Kirkwood to the east side of the Hope Valley graben; these are interpreted to occur across the central Sierra and record Miocene uplift events (Busby and Putirka 2009). We do not find the previously mapped unconformities 4 and 5 of Busby *et al.* (2008a) at Hope Valley, and do not consider them to be significant unconformities. Correlations of units across regions are noted by dashed lines; abbreviations include: conglomerate, cg; sandstone, ss; biotite, bt; hornblende, hb; and pyroxene, pyx.

The Relief Peak Formation was originally defined to apply only to calc-alkaline volcanic rocks that underlie 10–9 Ma high-K volcanic rocks of the Stanislaus Group found near Sonora Pass (Slemmons 1966; Busby *et al.* 2008b). Because no high-K rocks occur in the Carson Pass region, we follow previous workers by referring to andesitic volcanic and volcaniclastic rocks in the Carson Pass area as the Mehrten Formation (Piper *et al.* 1939; Curtis 1951, 1954; Wilshire 1956; Wagner and Saucedo 1990; Saucedo and Wagner 1992).

Mosier (1991) divided volcanic–volcaniclastic rocks in the Markleeville Peak–Jeff Davis Peak area (Figure 2(a)), where he recognized welded ignimbrites that he assigned to the Valley Springs Formation, as well as lahar deposits, andesitic lava flows, and dikes that he assigned to the Relief Peak Formation. While we agree with some of Mosier's interpretations of rock types and contacts, we differ in one important way. On Markleeville Peak, Mosier mapped a very thick sequence of lava flows, with the oldest interfingering with the Oligocene Valley Springs Formation and the youngest dated at 7 Ma. We reinterpret Markleeville Peak as a dacite to andesite intrusive complex that formed between about 6.3 and 6.14 Ma (Figure 2(a)).

Busby *et al.* (2008b) presented a preliminary, simplified geologic map of the Hope Valley Graben. Here, we present new geochemical and geochronologic data, modal analyses, and a more detailed geologic map. The new map includes correlations of fluvial and debris flow deposits across the graben and a chronostratigraphic column correlating units on the basis of age, petrography, and geochemistry (Figure 2(b)). We integrate these data with data published by Busby *et al.* (2008a) to construct a new sequence stratigraphic model for the evolution of the Kirkwood–Carson Pass–Hope Valley palaeocanyon system, and to interpret the history of the range-front faults at Carson Pass.

## Field studies

We divide Tertiary rocks into ignimbrites, block-and-ash-flow tuffs, debris-flow deposits, fluvial deposits, lava flows, and intrusions, and further divide primary volcanic and intrusive rocks by mineralogy and chemistry (Figure 2). Many contacts between basement rocks and the Tertiary rocks mapped by Armin *et al.* (1983, 1984) are retained with slight modifications described below. All Cretaceous plutonic rocks mapped by Armin *et al.* (1983, 1984) are grouped into one unit. All of the Quaternary deposits also are grouped into one unit, because there are no exposed fault scarps within these units. We reinterpreted some of the lithofacies in Mosier's (1991) MS thesis area, including some of his debris-flow units that we recognize as block-and-ash-flow tuffs and, as noted above, his lava flows, which we map as intrusions. We added more detail to the eastern edge of the Carson Pass–Kirkwood map published by Busby *et al.* (2008a), along the present-day Sierran crest at Elephant's Back and Red Lake Peak (Figure 2(a)). New correlations of map lithofacies and unconformities between the Carson Pass–Kirkwood area of Busby *et al.* (2008a) and the Hope Valley area (this study) are summarized in Figure 2(b). North–south and east–west cross-sections are shown in Figure 3. The stratigraphic section is divided into four sequences by geologic mapping and correlation of four unconformities within the palaeochannel fill (Figure 2(b)).

## $^{40}Ar/^{39}Ar$ dating

$^{40}Ar/^{39}Ar$ dating of key igneous units was performed at the Berkeley Geochronology Center. Methods used were similar to those reported by Verdel *et al.* (2007). Samples were generally ca. 10–20 mg multigrain aliquots of handpicked crystals from the 20–60 mesh size fractions. Samples were irradiated for 10 h in the CLICIT facility at the Oregon State

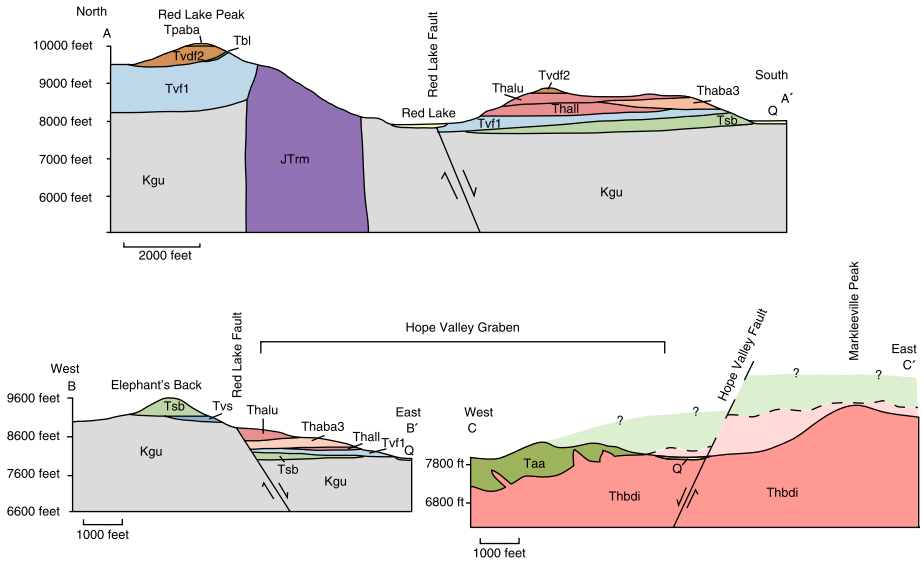


Figure 3. Geologic cross-sections through the Hope Valley Graben. (a) Cross-section A–A′ from north to south through Red Lake Peak, Red Lake, the Red Lake Fault, and the hills east of Elephant's Back. We correlate a fluvial unit (Tvf1) near the base of the palaeocanyon across the fault, and use it to estimate an offset of at least 365 m (1200 ft) across the fault. (b) Cross-section B–B′ from Elephant's Back on the Sierran crest eastwards, through the Red Lake Fault south of cross-section A–A′. The stratified cobble breccia–conglomerate of Elephant's Back (Tsb; Figure 2(a)) is offset at least 400 m (1300 ft). (c) Cross-section C–C′ through the Hope Valley Fault and Markleeville Peak. To the east of the fault, Markleeville Peak is an intrusive complex (Thbdi) that intrudes the palaeocanyon fill. We interpret the heavily altered rocks west of the fault (Taa) to represent the roof rocks to this intrusive complex, down-dropped along the Hope Valley Fault by about 370 m (1200 ft).

University TRIGA reactor, along with Fish Canyon sanidine (FCs) as a neutron fluence monitor. Stepwise degassing with a $CO_2$ laser beam steered through an integrator lens yielded the apparent age spectra (Figure 8).

All but two samples yielded well-defined age plateaux. Of the remaining eight samples, two with plateau ages indicated by an asterisk (*) failed to meet an arbitrary but commonly used criterion that plateaux should comprise three or more consecutive steps with ages mutually indistinguishable at 95% confidence, containing $>70\%$ of the $^{39}Ar$ released. These samples' departure from 'ideal' plateaux is minor and the plateau ages given are judged to be reliable. Age uncertainties are shown (Figure 8) at one standard deviation but discussed in the text at two standard deviations, and do not include contributions from uncertainties in decay constants or the age of the standard.

Ages are summarized in Table 3 both as 'nominal' and 'preferred' values. Nominal ages are based on an age of 28.02 Ma for FCs, as recommended by EARTHTIME community consensus. However, direct intercalibration of FCs with the astronomical time scale was recently accomplished (Kuiper *et al.* 2008), yielding an age of 28.201 Ma for FCs. We adopt this age herein to calculate the preferred ages shown in Table 3, which are believed to be more accurate and more appropriate for comparison with the astronomically calibrated geomagnetic polarity time scale of Gradstein *et al.* (2004). Consequently, preferred ages (based on FCs = 28.201 Ma) are used herein throughout, except in the nominal age column of Table 3.

## Tertiary volcanic, volcaniclastic, and intrusive suites

We define 23 Tertiary map units in the Hope Valley area (Figure 2), based on outcrop and thin section characteristics, described and interpreted in Table 1. Mappable units include intrusions, primary volcanic and volcaniclastic rocks (ignimbrites, lava flows, and block-and-ash-flow tuffs), and secondary volcaniclastic rocks (debris-flow deposits and fluvial deposits). The volcanic–volcaniclastic terminology used in this paper largely follows that of Fisher and Schminke (1984) and Heiken and Wohletz (1985). We assign lithofacies names based on compositions and mineralogy, sedimentary structures and textures, and inferred eruptive and depositional processes. Representative photographs of each of the lithofacies are shown in Figure 4. For convenience, the reader is referred to the sequence number in discussion of specific map units. Modal analyses for all of the intrusive and the primary volcanic–volcaniclastic map units are given in Figure 5, and geochemical data are given in Table 2 and Figure 6. Representative photomicrographs are shown in Figure 7. $^{40}Ar/^{39}Ar$ ages for intrusions and primary volcanic–volcaniclastic rocks are summarized in Table 3, and the spectra are shown in Figure 8. All errors given for ages in the text are $2\sigma$. The age data are presented together with the field, thin section, and geochemical description of each unit dated. Geochemical work was completed at Putirka's laboratory at California State University at Fresno, and the methods are described in Busby *et al.* (2008b).

### *Ignimbrites*

The oldest Tertiary rocks in the area are ignimbrites, referred to as the Valley Springs Formation, which are preserved within the Hope Valley–Carson Pass–Kirkwood palaeocanyon system (Figure 2; also see Figure 2 of Busby *et al.* 2008a). These rocks are found in palaeochannels throughout the Sierra Nevada and consist of silicic ignimbrites that erupted from Oligocene sources in central Nevada (Figure 9(a); Davis *et al.* 2000; Henry *et al.* 2003; Hinz *et al.* 2003; Garside *et al.* 2005). In our field area, these ignimbrites are preserved as thin deposits on palaeochannel floors and walls (Figure 9(b); Busby *et al.* 2008a,b; Busby and Putirka 2009) forming outcrops in the southeastern part of the field area, between Markleeville Peak and Jeff Davis Peak (Figure 2(a)). The outcrops contain sanidine, quartz, biotite, hornblende, lithic clasts, and pumice shards up to 1 cm in size in a grey–white ash matrix containing bubble-wall shards. The ignimbrites are weakly welded to non-welded. Mosier (1991) reported a sanidine K/Ar age of 28.2 ± 1.1 Ma for this unit, and Armin *et al.* (1983) reported a biotite K/Ar age of 25.9 ± 0.4 Ma on an ignimbrite which we re-map as ignimbrite clasts inside volcanic fluvial sandstone (Tvs) at the northwestern end of the field area.

### *Shallow-level intrusions*

We distinguished six intrusions or intrusive suites in the Hope Valley area (Figure 2) and report modal analyses (Figure 5), geochemical data (Figure 6; Table 2), and geochronological data (Figure 8; Table 3). They are described below from the oldest to the youngest.

The hornblende basaltic andesite Round Top intrusions (Tbai; Table 1) contain large hornblende glomerocrysts, locally in clots as large as 10 cm long. These distinctive glomerocrysts, coupled with resorbed plagioclase, indicate a complex magmatic history. Morton *et al.* (1977) reported a 13.4 ± 1.5 Ma K/Ar age for this intrusion. We found clasts containing these large hornblende glomerocrysts in many of the surrounding fluvial and debris-flow deposits.

Table 1. Description of lithofacies and intrusions for map units shown on Figure 2(b). Each Tertiary map unit is named and described through field observations and through petrographic observations.

| Unit label | Field description | Thin section description |
|---|---|---|
| Sequence 4 | | |
| Tri – Rhyolite intrusion | Cream-coloured rhyolite intrusion, with orange Liesegang bands. Plagioclase, hornblende, and quartz visible in hand sample. Closely spaced cleavage in three directions with highly variable orientations. Restricted to a single locality intruding altered andesites (Taa) | Presence of quartz and K-spar phenocrysts and geochemistry suggests rhyolitic composition, but clay alteration precludes meaningful geochronologic or modal analysis |
| Thadp – Hornblende andesite dike and plugs; 6.37 ± 0.24 Ma | Grey andesitic dikes and small plugs cutting Markleeville Peak dacite–andesite intrusions (Thbdi) and the altered andesite (Taa). Vertical platy fabric. Small phenocrysts of plagioclase and hornblende | Phenocrysts of plagioclase > hornblende and local microcrystalline biotite; phenocrysts proportions and percentages vary from dike to dike. Plag laths aligned parallel to dike margins |
| Thbdi – Markleeville Peak hornblende–biotite dacite and andesite intrusions. Dacite dated at 6.34 ± 0.14 Ma and andesite dated at 6.18 ± 0.14 Ma | Light grey to red biotite hornblende dacite to basaltic andesite. Hornblende commonly visible in hand sample, up to 2 × 4 mm. Biotite commonly visible, 1–2 mm, and euhedral. Some regions of intrusion are aphyric. Locally columnar jointed. Local horizontal joints spaced approximately 15 cm apart | Phenocrysts: plagioclase > biotite > hornblende. Zoned plagioclase (1–2 mm) with clay replacement in interior; smaller crystals of hb (0.5–1 mm), some altered to clay and weathered out, leaving holes. Local apatite and biotite inclusions in plag, and local groundmass apatite |
| Taa – Altered andesite | Extremely altered hornblende and plagioclase-rich lava flows, block-and-ash flow tuffs, and debris-flow deposits. Varies in colour from purple to blue to coppery-green with clasts frequently green, red, or white. Most plagioclase altered to clay, with epidote crystallization in some locations. Minor copper mineralization in area visible as bright green veins in rocks; Charred and silicified wood visible in one probable block-and-ash flow tuff | Phenocrysts: oxyhornblende rather than hornblende ≫ plagioclase which is partly or completely altered to sericite; abundance and size of phenocrysts vary; modal analysis difficult to useless due to heavy presence of clay |

Table 1 – *continued*

| Unit label | Field description | Thin section description |
|---|---|---|
| Tbi – Basalt intrusion | Black basalt intrusions at Sierran crest (in NW) and near Pickett Peak (in E). It has well-developed columnar joints at Pickett Peak, up to 40 cm wide, where it forms a large talus slope. Plagioclase and olivine (partially altered to iddingsite) visible in hand sample | Phenocrysts: plagioclase > olivine ≫ pyroxene; minor iddingsite alteration of olivine; groundmass very fine-grained with plagioclase laths and olivine |
| Thbai – Horsethief Canyon hornblende–biotite andesite intrusion | Columnar jointed dark grey to black hornblende–biotite andesite intrusion; columns ~ 1 m wide, with horizontal jointing radiating away from the joints. Large intrusion at peak that continues as an ~ 40 m (130 ft) wide dike at 310° to NW. Second, dike of same composition and similar width and characteristics outcrops to N, also trending 310° | Hornblende (up to 3 mm) and biotite (up to 1.5 mm) crystals, plagioclase slightly altered to clay. Biotite rims slightly oxidized, 60% of hornblende oxidized |
| Thai – Steven's Peak hornblende basaltic andesite intrusion | Large plug with abundant columnar jointing; very altered, with clay replacement of plagioclase, and bluish-grey hornblende. Dated by K/Ar at 5.2 ± 0.8 Ma (McKee oral commun. in Armin *et al.* 1984); too altered to sample for Ar/Ar dating | Altered phenocrysts of hornblende up to 3 mm ≫ plagioclase in a fine-grained plagioclase-rich plus cpx groundmass; clay makes up ~ 10% of the sample |
| Tpaba – Red Lake Peak pyroxene basaltic andesite block-and-ash-flow tuff; 6.29 ± 0.1, 6.13 ± 0.34 Ma | Dark grey to black andesite, with glassy blocks in a lapilli tuff matrix of the same composition, unsorted, and massive to very crudely stratified. Glomerocrysts of clinopyroxene. Two pyroxenes visible in hand sample | Phenocrysts: plagioclase > hornblende > clinopyroxene > orthopyroxene; hornblende has thick oxidized rims. Both pyroxenes are euhedral, up to 3–4 mm; plagioclase has opaque inclusions. Groundmass glassy with square plagioclase microlites |
| Tvdf2 – Volcaniclastic debris flow deposit; Little Round Top debris flow deposit of Busby *et al.* (2008a) | Tan deposit composed of sub-rounded to sub-angular, pebble–boulder (up to 1.5 m) volcanic clasts in a coarse sand matrix. Clasts poorly sorted, unstratified, in a massive deposit. Clasts of hornblende–plagioclase andesite with minor mafic and granitic clasts. A megablock of flow-banded lava (> 30 m wide) with similar geochemistry to unit Tpai found inside the upper debris-flow east of Elephant's Back | See Tvdf1 |

Table 1 – *continued*

| Unit label | Field description | Thin section description |
|---|---|---|
| Thalu – Upper hornblende andesite lava flow | Reddish-tan andesite lava flow, with a 4 m thick basal breccia and a 100 m (300 ft) thick coherent, columnar jointed interior. Abundant large hornblendes, up to 1 cm. Unaltered. Accidental clasts of other andesites mixed into basal breccia. A 10 m wide, 10 m thick lens of hornblende andesite block and ash flow tuff overlies this flow at one locality | Similar composition and relative abundance of minerals as Thall, but hornblende crystals are slightly larger, up to 6 mm |
| Thaba3 – Hornblende andesite block-and-ash-flow tuff | Purple to white hornblende andesite, with glassy blocks and lapilli (up to 50 cm), supported in a crystal and ash matrix of same composition, massive, and unsorted. Forms a lens between the lower and upper andesite lava flows. Clasts sub-angular to angular, with bread-crust texture, radial jointing, and *in situ shattering of blocks.* Matrix locally yellowish-green and purple | Plagioclase > hornblende in a glassy groundmass with plag microlaths; 80% of hornblende is altered to oxy-hb or clay; only 3% of plagioclase is altered to clay |
| Thall – Lower hornblende andesite lava flow; 6.22 ± 0.14 Ma | Reddish-tan hornblende andesite lava flow, lower of two flows. Generally smaller crystals than upper flow, especially hornblende. Very prominent bench marks contact between lava flow and fluvial section below. Flow has basal breccia 1–3 m thick, and coherent interior at least 60 m (200 ft) thick, with columnar joints 20 cm wide. Flow-top breccia only ~ 1 m thick or not exposed; flow top marked by a prominent bench | Euhedral plagioclase > hornblende, in unaltered microcrystalline groundmass. Hornblende rims altered. Plagioclase up to 6 mm; hornblende up to 4 m, common large = 1.5 × 3 mm and common small = 0.25–0.5 mm |

Table 1 – *continued*

| Unit label | Field description | Thin section description |
|---|---|---|
| Tbl – Basalt lava flows | Black, glassy, aphyric to crystalline basalt lava flows. Up to five flows, each 2–3 m thick; aphyric to olivine- and plagioclase-phyric. Vesicular and/or brecciated horizons occur at the top of each flow | Phenocrysts of iddingsitized olivine $\gg$ clinopyroxene and plagioclase; groundmass of plagioclase with minor olivine |
| Sequence 3 | | |
| Tvf2 – Volcanic fluvial conglomerates and sandstones | Tan to grey cliff-forming pebble to cobble conglomerate and pebbly sandstone, with sub-rounded to rounded clasts. Well-sorted, well stratified, thin to medium bedded, with planar lamination and trough cross-lamination. Fills channels cut into underlying debris-flow deposit (Tvdf 1), restricted to hills north of Charity Valley in SE | Same as Tvf1 |
| Tpai – Pickett Peak and Hawkins Peak pyroxene andesite intrusion; 10.77 ± 0.10 Ma | Dark grey to black andesite plugs that make up the peaks of Pickett and Hawkins Peak. Well-developed columnar joints throughout, up to 2 m wide. Plugs up to 350 m (1150 ft) wide, with two-pyroxenes (both cpx and opx) visible in hand sample, and some cpx glomerocrysts | Crystal-rich (35–50% crytsals). Plag > clinopyroxene = orthopyroxene. Round oxide crystals inside and surrounding cpx; sericite rims on plag. Some opx crystals have rims of microcrystalline cpx. Plag has inclusions of opx, and plag commonly grows in clusters around cpx (Figure 7(A)). Samples from the base of Hawkins Pk have same crystal intermixing of plag and pyx, but also contain hornblende (sample 71; Figure 5) |
| Tvdf1 – Volcaniclastic debris-flow deposit; age ≧ 10.72 ± 0.12 Ma (WR date on andesite dike with peperite margins; Busby *et al.* 2008a) | Tan, poorly sorted, matrix-supported, massive to indistinctly stratified cobble to boulder breccia with sub-rounded to angular clasts, in a pebbly sandstone matrix. Dominated by hornblende and pyroxene andesite clasts, up to 2 m in size, with minor olivine basalt and granitic clasts | Thin section characteristics of debris-flow sandstone matrix similar to that of sandstones in fluvial units |

Table 1 – *continued*

| Unit label | Field description | Thin section description |
|---|---|---|
| Tvf1 – Volcanic fluvial conglomerates and sandstones | Tan to grey, stratified, clast-supported cobble conglomerate and lesser pebbly/cobbly sandstone; moderately well-sorted with sub-angular to rounded clasts, in medium to thick beds with planar lamination and cut-and-fill structures. Unit commonly coarsens upwards. Cliff-forming, especially at the Sierran crest, where it also has lesser debris-flow deposits. Clasts include hornblende and pyroxene andesites, with minor granite and basaltic clasts, up to 50 cm in size. A sandstone-rich base passes gradationally upwards into progressively coarser and less well-sorted conglomerates, with progressively more crude stratification, with fewer and more lenticular sandstone interbeds, and more angular clasts upsection | Thin section characteristics of sandstone beds and sandstone matrix characteristics very similar to unit Tvs; contains rounded clasts and crystals of probable Tertiary volcanic origin 0.2–0.5 mm |
| Sequence 2 | | |
| Thaba2 – Red Lake Peak hornblende andesite block-and-ash-flow tuff; 13.5 ± 0.16 Ma | Angular and shattered blocks of light pink plag- and hornblende-phyric andesite with blocks in an ash matrix of the same composition. Massive and unsorted, generally matrix-supported. Blocks slightly vary in colour from white to grey to pink, but retain same phenocryst assemblage | Plagioclase > hornblende ≫ biotite > orthopyroxene in glassy groundmass; plagioclase has some hornblende and apatite inclusions |
| Thaba1 – Carson Pass trachyandesite block- and-ash-flow tuff and interstratified debris-flow deposits; 15.01 ± 0.06 Ma (Busby *et al.* 2008a) | Blocks of white, glassy, hornblende + biotite andesite in an ash matrix of same composition. Massive and unsorted. Prismatic jointing and bread-crust texture on blocks, as well as charring of petrified wood, indicate hot deposition | Phenocrysts: hornblende > plagioclase > biotite; groundmass: glass ≫ plagioclase microlites (Busby *et al.* 2008a) |

Table 1 – *continued*

| Unit label | Field description | Thin section description |
|---|---|---|
| Tphaba – Jeff Davis Peak pyroxene–hornblende andesite and dacite block-and-ash-flow tuffs; 15.5 ± 0.6 Ma | Reddish-tan plagioclase hornblende andesite block and lapilli fragments in a tuff matrix of the same composition. Massive and unsorted. Propylitically altered with some copper mineralization (aqua-green coating); commonly oxidized | Plagioclase ≫ clinopyroxene > orthopyroxene > hornblende. Hb has oxy-hb rims. Groundmass holocrystalline (80% plag laths) to altered glass |
| Tbai – Round Top hornblende basaltic andesite; 13.4 ± 1.5 Ma (Morton *et al.* 1977) | Tan to grey cliff-forming intrusion. Hornblende crystals and hornblende glomerocrysts up to 1–2 cm, locally up to tens of centimetres in size. Locally vesiculated horizons | Hornblende > plagioclase; trace clinopyroxene and oxides. Hb has thin oxy-hb rims. Holocrystalline groundmass. Larger plagioclase phenocrysts resorbed |
| Tsb – Elephant's Back stratified cobble breccia–conglomerate | Black to grey, moderately well-sorted, crudely stratified, sub-angular to sub-rounded, clast-supported pebble- to small-cobble breccia/conglomerate. Minor interbedded sandstone and siltstone. Clasts of andesite to basalt | No sandstone matrix (clast-supported) |
| Tvs – Volcanic fluvial sandstones. Elephant's Back sandstone in Busby *et al.* (2008a), but extends across the Hope Valley area. Intruded by Round Top basaltic andesite intrusion (13.4 ± 1.5 Ma; Morton *et al.* 1977) | Pebbly volcanic sandstone, tan, with largely andesite clasts, but includes Valley Spring Fm ignimbrite clasts at Horsethief Canyon (in NE) and just west of the Sierran crest (in NW). Sandstone matrix, coarse-grained, and lesser medium-grained, with volcanic rock fragments and lesser grains of quartz, plagioclase, and biotite. Predominately medium- to thin-bedded, locally massive, with cut-and-fill structures, planar lamination and medium- to large-scale trough cross-lamination | Sandstone matrix dominated by intermediate-composition volcanic rock fragments. Minor mineral grains of probable Tertiary volcanic origin include sub-euhedral quartz, sub-euhedral plagioclase, and rounded pyroxene. Minor mineral grains of probable granitic basement provenance include rounded quartz and rounded potassium feldspar. Opaque minerals locally abundant and aphyric basaltic clasts |
| Sequence 1 | | |
| Ti – Valley Springs Formation; age dated from 28.2 (Mosier 1991) to 23 Ma (Busby *et al.* 2008a) | Welded to non-welded ignimbrite with sanidine, quartz, biotite, hornblende; flattened pumice and lithic rock fragment including rhyolite in an ash matrix; percentage of clasts and phenocrysts variable | Euhedral quartz and sanidine, ± biotite, and/or hornblende. Bubble-wall shards, glassy throughout sample |

A

B

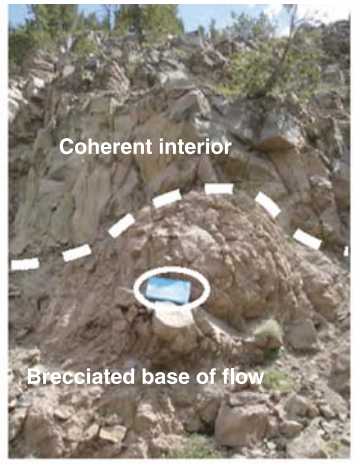
Coherent interior
Brecciated base of flow

C

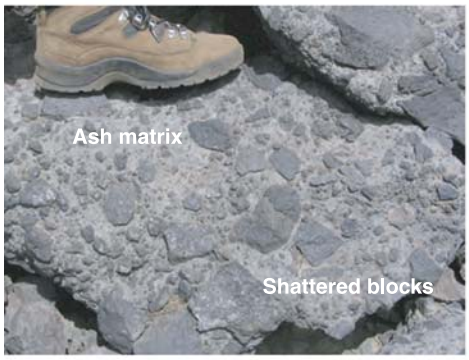
Ash matrix
Shattered blocks

D

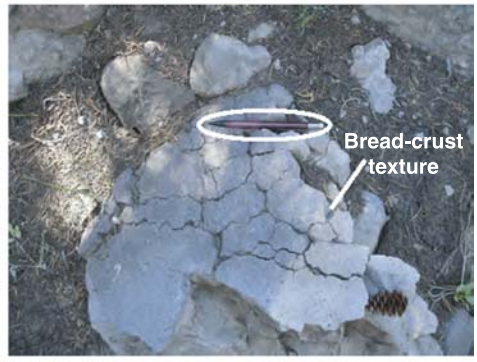
Bread-crust
texture

E

Reddened
base of flow
14 Ma block-and-ash flow

F

G

H

I

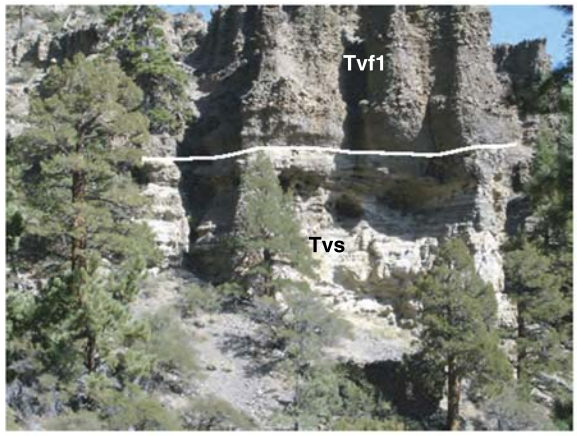


J

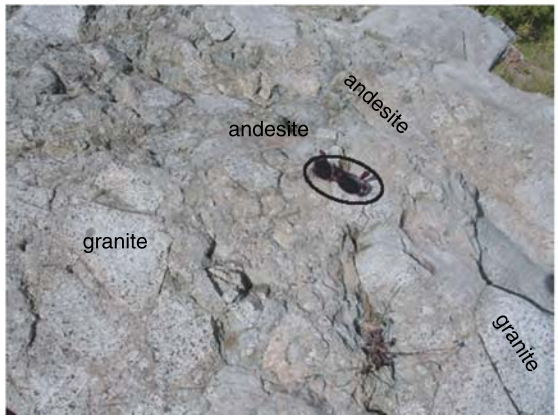

The 10.77 ± 0.10 Ma (Figure 8(d); Table 3) two pyroxene andesite plugs of Pickett Peak and Hawkins Peak (Tpai; Table 1) are identical in composition and mineralogy (Figure 5 and Table 3). The plugs are up to 300 m in diameter (Figure 4(a)). In thin section (Figure 7(a)), clinopyroxene and orthopyroxene are present in subequal amounts, subordinate to plagioclase (Figure 5), and plagioclase commonly grows in clusters around clinopyroxene (Figure 7(a)).

The 6.34 ± 0.14 to 6.18 ± 0.14 Ma (Figure 8(i,j); Table 3) hornblende–biotite dacitic and andesitic intrusions of Markleeville Peak (Thbdi; Table 1) cross-cut the southeastern palaeocanyon tributary (Figure 2), and consist of complex multiple plugs of irregular shape and composition that we did not attempt to map individually. They range from dacite to basaltic andesite in composition and contain varying amounts of hornblende, biotite, and plagioclase phenocrysts (Figures 5 and 6; Table 2). As noted above, these were mapped previously as Oligocene to late Miocene lava flows by Mosier (1991), but they clearly intrude Oligocene to late Miocene strata, and lack features typical of lava flows (described below). Small hornblende andesite dike and plugs intrude the hornblende–biotite andesites and dacites on top of Markleeville Peak (Thadp). A sample of one of these hornblende andesite dikes from the top of Markleeville Peak yielded an age of 6.37 ± 0.24 Ma (Figure 8(g); Table 3), which is indistinguishable from the age of the main Markleeville Peak plugs (Thbdi) that they intrude.

A small undated olivine basaltic andesite intrusion (Tbi; Table 1) intrudes sequence 3 debris-flow deposits on Pickett Peak (Figure 2). The olivine has been partially altered to iddingsite. We also mapped a small olivine basalt intruding fluvial deposits (Tvf1) on the NE Sierran crest (Figures 2, 5, and 6).

Figure 4. Representative photos of lithofacies described in Table 1. (a) Distinctive columnar joints in the 10.77 ± 0.10 Ma intrusions of Pickett Peak (Tpai); the western of the two plugs is shown here. Height of outcrop in the centre of the image is approximately 200 ft. (b) Hornblende andesite lava flow with basal flow breccia and coherent, faintly columnar jointed interior. Photograph taken just south of Red Lake (Thalu; Figure 2(a)). (c) Pyroxene andesite block-and-ash-flow tuff, with monolithic, angular non-vesicular (dense) clasts set in a matrix of ash-sized material of the same composition. Photo taken on Red Lake Peak (Tpaba; Figure 2(a)). (d) Andesite block with well-developed, delicate bread-crust texture indicating deposition while still hot. Photograph taken of block-and-ash-flow tuff at the base of map unit Tvdf2 (east of Elephant's Back; Figure 2(a)). (e) 6.29 ± 0.10 to 6.13 ± 0.34 Ma Red Lake Peak pyroxene andesite block-and-ash-flow tuff (Tpaba) with oxidized basal interval, resting directly upon 13.61 ± 0.16 Ma Red Lake Peak hornblende andesite block-and-ash-flow tuff (Thaba2), on the north face of Red Lake Peak. (f) Massive, unsorted, coarse-grained volcanic debris-flow deposit with a variety of angular to sub-rounded andesite clast types, supported by a buff pebbly sandstone matrix (Tvdf2 east of Elephant's Back). (g) Crudely stratified, clast-supported deposit, with sedimentary structures and textures transitional between those of debris-flow deposits and fluvial deposits; mapped as a debris-flow deposit throughout the field area. Photograph taken at the base of map unit Tvdf1 west of Pickett Peak. (h) Well-stratified and well-sorted fluvial deposit, with planar-laminated and cross-laminated beds and rounded clasts of a variety of types of andesite. Photo taken from map unit Tvf1 above Crater Lake on the Sierran crest. (i) The contact between the white, ignimbrite-clast rich well-stratified pebbly sandstone (Tvs) and the light brown, pebble to cobble crudely stratified fluvial conglomerate and sandstone (Tvf1). Photograph taken from Horsethief Canyon, looking east. (j) Brecciated Cretaceous granitic rock, intruded by a plagioclase andesite porphyry. This granite breccia forms an approximately 200 m-long and 40 m-wide elongate pod that lies along the Red Lake Fault zone between Elephant's Back and Blue Lake, where the fault zone forms a southward-widening zone of brecciated granite with calcite veins (Figure 2(a), indicated by wavy lines).

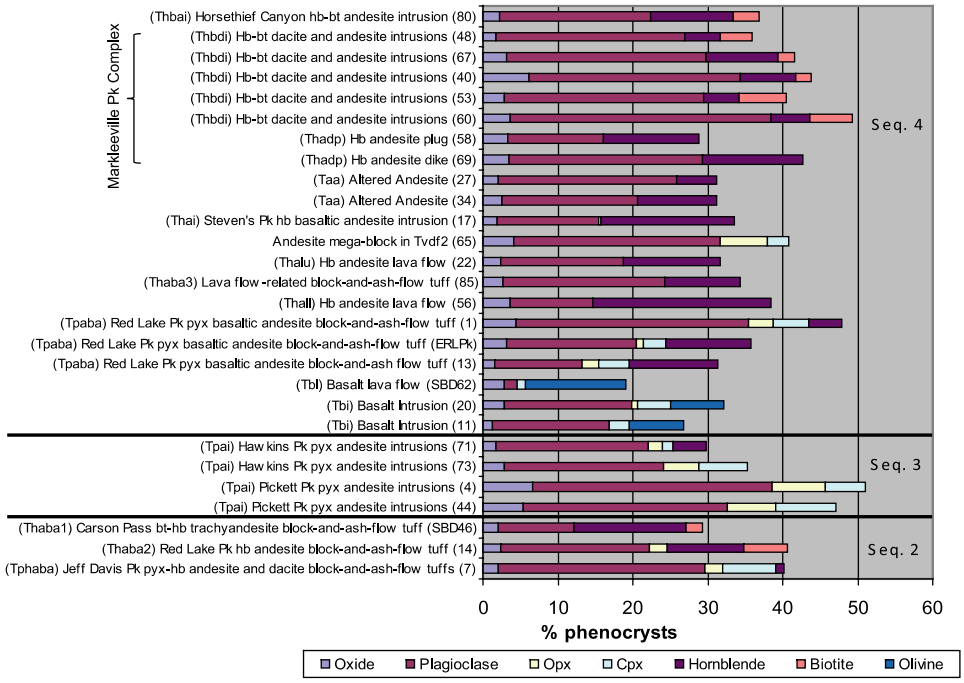
Markleeville Pk Complex
(Thbai) Horsethief Canyon hb-bt andesite intrusion (80)
(Thbdi) Hb-bt dacite and andesite intrusions (48)
(Thbdi) Hb-bt dacite and andesite intrusions (67)
(Thbdi) Hb-bt dacite and andesite intrusions (40)
(Thbdi) Hb-bt dacite and andesite intrusions (53)
(Thbdi) Hb-bt dacite and andesite intrusions (60)
(Thadp) Hb andesite plug (58)
(Thadp) Hb andesite dike (69)
(Taa) Altered Andesite (27)
(Taa) Altered Andesite (34)
(Thai) Steven's Pk hb basaltic andesite intrusion (17)
Andesite mega-block in Tvdf2 (65)
(Thalu) Hb andesite lava flow (22)
(Thaba3) Lava flow-related block-and-ash-flow tuff (85)
(Thall) Hb andesite lava flow (56)
(Tpaba) Red Lake Pk pyx basaltic andesite block-and-ash-flow tuff (1)
(Tpaba) Red Lake Pk pyx basaltic andesite block-and-ash-flow tuff (ERLPk)
(Tpaba) Red Lake Pk pyx basaltic andesite block-and-ash flow tuff (13)
(Tbl) Basalt lava flow (SBD62)
(Tbi) Basalt Intrusion (20)
(Tbi) Basalt Intrusion (11)
(Tpai) Haw kins Pk pyx andesite intrusions (71)
(Tpai) Haw kins Pk pyx andesite intrusions (73)
(Tpai) Pickett Pk pyx andesite intrusions (4)
(Tpai) Pickett Pk pyx andesite intrusions (44)
(Thaba1) Carson Pass bt-hb trachyandesite block-and-ash-flow tuff (SBD46)
(Thaba2) Red Lake Pk hb andesite block-and-ash-flow tuff (14)
(Tphaba) Jeff Davis Pk pyx-hb andesite and dacite block-and-ash-flow tuffs (7)
Seq. 4
Seq. 3
Seq. 2
0
10
20
30
40
50
60
% phenocrysts
Oxide
Plagioclase
Opx
Cpx
Hornblende
Biotite
Olivine

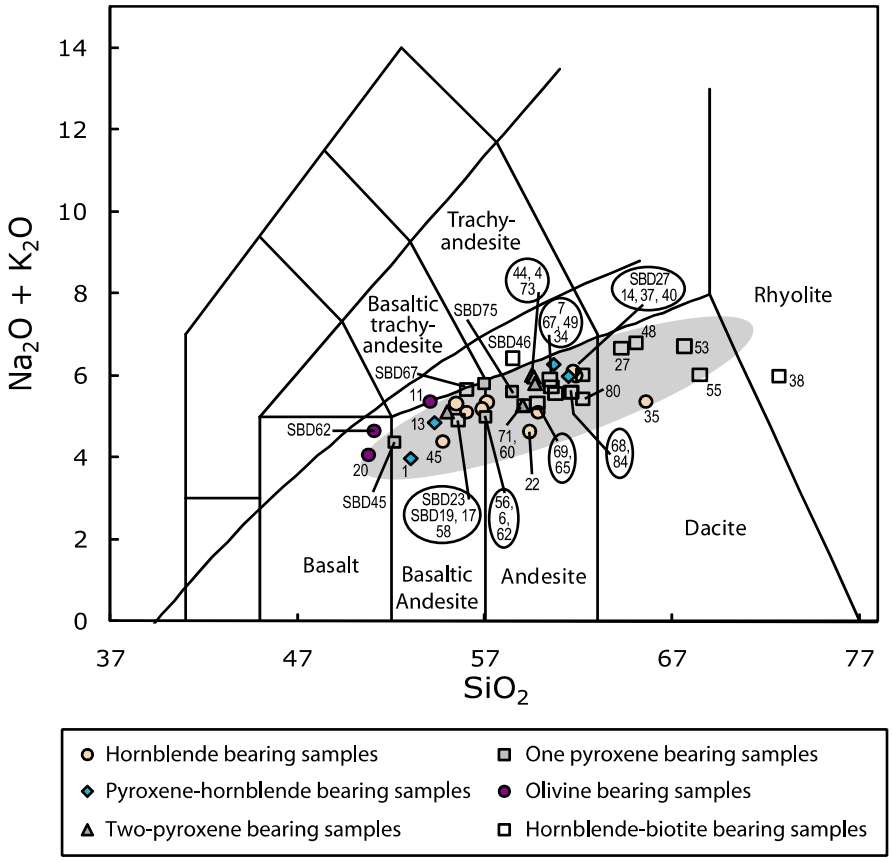
$Na_2O + K_2O$
$SiO_2$
0
2
4
6
8
10
12
14
37
47
57
67
77
Trachy-andesite
Basaltic trachy-andesite
Rhyolite
Basalt
Basaltic Andesite
Andesite
Dacite
SBD75
SBD46
SBD67
SBD62
SBD45
SBD27 14, 37, 40
SBD23 SBD19, 17 58
44, 4 73
7 67, 49 34
71, 60
69, 65
68, 84
56, 6, 62
48
53
27
55
38
35
80
22
11
13
45
1
20
Hornblende bearing samples
Pyroxene-hornblende bearing samples
Two-pyroxene bearing samples
One pyroxene bearing samples
Olivine bearing samples
Hornblende-biotite bearing samples

Figure 5. Modal analyses of primary volcanic deposits and intrusions in the Hope Valley area. Map unit names, symbols, and sequence numbers correspond to Figure 2 and Table 1. Sequence 2 has three block-and-ash-flow tuffs, sequence 3 has one intrusive suite, and sequence 4 has the rest of the primary volcanic and intrusive rocks, arranged here in order of increasing silica content from bottom to top (Table 3; Figure 6). All samples geochemically analysed except ERLPk and sample 85. One thin section per analysis with 1000 counts per thin section; GPS localities given in Table 2.

A hornblende basaltic andesite intrudes strata (map units Tvf1 and Tvdf2) at Steven's Peak (Thai; Table 1). It has a reported K/Ar age of 5.2 ± 0.8 Ma (Armin *et al.* 1984), but due to alteration we were unable to find phenocrysts suitable for $^{40}Ar/^{39}Ar$ dating.

The larger shallow-level intrusions in the map area could be easily mistaken for thick sequences of lava flows, but they differ from lava flows in several ways. Erosional benches are well developed in both the Round Top and Markleeville Peak intrusions, but they are less continuous and less prominent than those formed in lava flow sections, and lack the laterally continuous vesiculated tops of lava flows. Although the intrusions may be locally brecciated, the breccias lack the lateral continuity of flow-top breccias. Columnar jointing is common in both lava flows and intrusions, but the intrusions commonly have thin (<5 cm thick) horizontal joints that resemble flow banding.

To summarize, most of the shallow-level intrusions, except for the 8 km-diameter Markleeville Peak Center, are small (<2 km across). They range from basalt to two pyroxene andesite through hornblende andesites to hornblende–biotite dacites. They were emplaced at about 14 Ma (hornblende andesite), about 11 Ma (two pyroxene andesites), and about 6 Ma (hornblende–biotite andesites and dacites and hornblende andesites). The small basalt plugs are undated. Although the number of intrusions is small, there does not appear to be any temporal trend in compositions.

### *Lava flows*

Lava flows are much less common than fragmental rocks in the Carson Pass–Markleeville region, as first noted by Curtis (1951, 1954). We mapped two lava flow sections in the Carson Pass–Hope Valley area: (1) sequence 4 basalt lava flows (Tbl) on the Sierran crest, dated at 6.80 ± 0.20 Ma by Busby *et al.* (2008a), recalculated to our preferred age of 6.95 ± 0.20 Ma (Table 3) and (2) sequence 4 hornblende andesite lava flows (Thall and Thalu) deposited on the footwall of the Red Lake Peak Fault (Figures 2 and 3) here dated at 6.22 ± 0.14 Ma (Figure 8(h); Table 3).

The basalt lava flow (Tbl; Table 1) section is variable in thickness, because it onlaps unconformity surface 4 (unconformity 6 of Busby *et al.* 2008a; Figure 2). It consists of two to five flows, 2–6 m thick, which are mainly aphyric, with one containing olivine and plagioclase phenocrysts. The top of each flow is marked by breccia or by a vesicular horizon, and the flow interiors are columnar jointed.

The andesite lava section lies inside the Hope Valley Graben, and consists of two very thick lava flows separated by a block-and-ash-flow tuff (Thaba3; Figure 2; Table 1), referred to as the lower and upper hornblende andesite lava flows (Thall and Thalu; Figure 2; Table 1). A topographic bench marking the contact between the underlying

Figure 6. Alkali–silica (Le Bas *et al.* 1986) classification diagram for the Kirkwood Valley–Carson Pass–Hope Valley volcanic rocks and intrusions. Open circle represents present-day calc-alkaline Cascades arc volcanism from Lassen data (Clynne 1990). Data and GPS coordinates are given in Table 2. Locations for samples labelled SBD# are plotted in Figure 2 of Busby *et al.* (2008a). Organized by mineralogy; colour and shape of symbol indicates the presence of identifying minerals.

Table 2. Geochemical analyses from primary volcanic rocks (lava flows and block-and-ash-flow tuffs), intrusions, and lesser clasts within debris-flow deposits, Hope Valley–Carson Pass–Kirkwood area.

| Unit | Pheno | Sample # | $SiO_2$ | $TiO_2$ | $Al_2O_3$ | $Fe_2O_3$ | MnO | MgO | CaO | $Na_2O$ | $K_2O$ | Cr (ppm) | $P_2O_5$ | Sum | Rock name | Lat (°N) | Long (°W) |
|---|---|---|---|---|---|---|---|---|---|---|---|---|---|---|---|---|---|
| Thai | hb | JHCP-17 | 55.44 | 0.91 | 19.11 | 8.07 | 0.1 | 3.45 | 7.48 | 3.19 | 2.02 | 20.5 | 0.355 | 100.3 | Basaltic andesite | 38.73492 | 119.98086 |
| Tvdf2[1] | hb | JHCP-65 | 59.1 | 0.79 | 18.55 | 6.51 | 0.07 | 2.66 | 6.26 | 3.39 | 2.17 | 1.6 | 0.269 | 99.77 | Andesite | 38.68648 | 119.97732 |
| Tvdf2[2] | hb | JHCP-22 | 59.41 | 0.81 | 19.23 | 6.56 | 0.07 | 2.46 | 6.5 | 2.64 | 2.01 | 15.9 | 0.269 | 99.96 | Andesite | 38.69024 | 119.97776 |
| Thall | hb | JHCP-56 | 57.12 | 0.8 | 18.31 | 7.09 | 0.09 | 3.54 | 7.21 | 3.45 | 1.91 | 49.5 | 0.334 | 99.86 | Andesite | 38.69089 | 119.97985 |
| Thalu | hb | JHCP-6 | 56.85 | 0.85 | 18.14 | 6.97 | 0.1 | 2.65 | 9.18 | 3.4 | 1.79 | 115.6 | 0.315 | 100.26 | Basaltic andesite | 38.68447 | 119.97476 |
| Tphaba | hb | JHCP-35 | 65.52 | 0.695 | 16.025 | 5.655 | 0.16 | 0.84 | 5.185 | 3.19 | 2.345 | 10 | 0.2735 | 99.89 | Dacite | 38.64393 | 119.90493 |
| Tvdf1[1] | hb | JHCP-45 | 54.78 | 1.11 | 17.95 | 8.17 | 0.1 | 5.2 | 7.97 | 2.71 | 1.7 | 77 | 0.298 | 100.00 | Basaltic andesite | 38.75189 | 119.89188 |
| Tvdf1[3] | hb | JHCP-37 | 61.85 | 0.62 | 18.08 | 5.4 | 0.05 | 2.95 | 5.16 | 3.61 | 2.39 | – | 0.232 | 100.34 | Andesite | 38.63137 | 119.89163 |
| Tbai | hb | SBDCP23 | 55.47 | 0.94 | 18.46 | 7.6 | 0.09 | 3.99 | 7.67 | 3.82 | 1.5 | 0 | 0.3 | 99.84 | Basaltic andesite | 38.66756 | 120.00164 |
| Taba2[**] | hb | SBDCP27 | 61.73 | 0.56 | 18.37 | 5.42 | 0.04 | 1.58 | 5.73 | 4.09 | 2.02 | 0 | 0.329 | 99.87 | Andesite | 38.41180 | 120.03382 |
| Thaba2 | opx–hb–bt | JHCP-14 | 61.46 | 0.73 | 17.39 | 5.25 | 0.06 | 3.47 | 5.72 | 3.29 | 2.7 | 60.3 | 0.265 | 100.34 | Andesite | 38.71842 | 119.98533 |
| Tphaba | 2pyx–hb | JHCP-7 | 60.67 | 0.81 | 18.09 | 5.52 | 0.04 | 2.84 | 5.98 | 4.02 | 2.26 | 27.7 | 0.301 | 100.53 | Andesite | 38.64326 | 119.90369 |
| Tpaba | 2pyx–hb | JHCP-1 | 53.05 | 1.23 | 19.11 | 8.93 | 0.5 | 3.13 | 10.06 | 2.65 | 1.335 | 40.9 | 0.322 | 100.32 | Basaltic andesite | 38.71388 | 119.98658 |
| Tpaba | 2pyx–hb | JHCP-13 | 54.32 | 1 | 19.46 | 7.51 | 0.09 | 3.13 | 8.82 | 3.05 | 1.81 | 49.2 | 0.36 | 99.55 | Basaltic andesite | 38.71224 | 119.98561 |
| Tpai | 2pyx | JHCP-44 | 59.49 | 0.87 | 17.2 | 6.21 | 0.06 | 3.95 | 6.35 | 3.51 | 2.49 | 38 | 0.316 | 100.45 | Andesite | 38.75435 | 119.89691 |
| Tpai | 2pyx | JHCP-4 | 59.6 | 0.84 | 17.28 | 6.19 | 0.06 | 3.81 | 6.33 | 3.44 | 2.52 | 40.8 | 0.31 | 100.38 | Andesite | 38.75678 | 119.90254 |
| Tpai | 2pyx | JHCP-73 | 59.66 | 0.89 | 17.52 | 6.11 | 0.06 | 3.58 | 6.32 | 3.34 | 2.46 | 48.7 | 0.315 | 100.26 | Andesite | 38.73818 | 119.87119 |
| Tpai | 2pyx | JHCP-71 | 58.3 | 0.82 | 18.21 | 6.8 | 0.1 | 3.16 | 6.58 | 3.33 | 2.08 | 33 | 0.297 | 99.68 | Andesite | 38.73956 | 119.87576 |
| Taba3[**] | 2pyx | SBDCP19 | 54.95 | 1.05 | 18.12 | 7.7 | 0.09 | 3.69 | 8.63 | 3.27 | 1.85 | 19.3 | 0.289 | 99.64 | Basaltic andesite | – | – |
| Tvdf2[3**] | pyx | SBDCP63 | 56.94 | 0.96 | 17.57 | 6.57 | 0.09 | 3.6 | 6.95 | 3.16 | 2.64 | 24.3 | 0.334 | 98.82 | Andesite | 38.71470 | 120.02381 |
| Tpaba | cpx | SBDCP45 | 52.18 | 1.2 | 18.36 | 9.09 | 0.21 | 3.72 | 10.32 | 3.1 | 1.28 | 40.7 | 0.327 | 99.79 | Basaltic andesite | 38.71406 | 119.98744 |
| Taba3[**] | cpx | SBDCP75 | 58.43 | 0.82 | 17.91 | 7.07 | 0.09 | 3.07 | 6.43 | 3.31 | 2.3 | 4.3 | 0.271 | 99.70 | Andesite | 38.70183 | 120.10372 |

Table 2 – *continued*

| Unit | Pheno | Sample # | $SiO_2$ | $TiO_2$ | $Al_2O_3$ | $Fe_2O_3$ | MnO | MgO | CaO | $Na_2O$ | $K_2O$ | Cr (ppm) | $P_2O_5$ | Sum | Rock name | Lat (°N) | Long (°W) |
|---|---|---|---|---|---|---|---|---|---|---|---|---|---|---|---|---|---|
| Tvdf2[3]** | pyx | JHCP-62 | 57.01 | 0.96 | 18.27 | 7.47 | 0.08 | 3.52 | 7.32 | 3.13 | 1.85 | 13.5 | 0.312 | 99.92 | Andesite | 38.73349 | 120.03360 |
| Tbi | cpx–ol | JHCP-11 | 54.04 | 1.12 | 19.28 | 8.09 | 0.09 | 4.08 | 7.41 | 3.43 | 1.93 | 23.2 | 0.275 | 99.75 | Basaltic andesite | 38.76260 | 119.90861 |
| Tbi | cpx–ol | JHCP-20 | 50.81 | 1.12 | 15.83 | 9.09 | 0.11 | 8.91 | 9.59 | 2.32 | 1.76 | 424.4 | 0.322 | 99.90 | Basalt | 38.74205 | 119.97841 |
| Tbl | cpx–ol | SBDCP62 | 51.11 | 1.03 | 15.71 | 8.99 | 0.12 | 8.58 | 9.36 | 2.96 | 1.7 | 0 | 0.328 | 99.89 | Basalt | 38.71008 | 120.01867 |
| Thbai | hb–bt | JHCP-80 | 62.21 | 0.9 | 18.21 | 5.9 | 0.05 | 2.35 | 5.1 | 3.13 | 2.32 | 57.1 | 0.267 | 100.44 | Andesite | 38.81280 | 119.86133 |
| Thbdi | hb–bt | JHCP-58 | 55.54 | 1 | 18.54 | 7.6 | 0.1 | 3.695 | 8.255 | 3.1 | 1.82 | 26.55 | 0.323 | 99.98 | Basaltic andesite | 38.65911 | 119.89582 |
| Thbdi | hb–bt | JHCP-40 | 62.23 | 0.6 | 18.37 | 5.18 | 0.04 | 1.72 | 6.1 | 3.84 | 2.18 | – | 0.284 | 100.54 | Andesite | 38.64469 | 119.89967 |
| Thbdi | hb–bt | JHCP-48 | 65.08 | 0.46 | 17.97 | 3.93 | 0.07 | 1.38 | 4.49 | 4.11 | 2.7 | 2.1 | 0.248 | 100.44 | Dacite | 38.67296 | 119.91543 |
| Thbdi | hb–bt | JHCP-53 | 67.64 | 0.34 | 17.24 | 3.1 | 0.07 | 0.95 | 3.76 | 4.08 | 2.65 | – | 0.152 | 99.98 | Dacite | 38.65813 | 119.92328 |
| Thbdi | hb–bt | JHCP-67 | 59.73 | 0.72 | 18.16 | 5.66 | 0.09 | 2.88 | 6.23 | 3.67 | 2.27 | 12 | 0.297 | 99.71 | Andesite | 38.65995 | 119.89956 |
| Thbdi | hb–bt | JHCP-60 | 59.015 | 0.805 | 18.665 | 6.2 | 0.07 | 2.58 | 6.785 | 3.52 | 1.885 | 6.3 | 0.307 | 99.83 | Andesite | 38.66105 | 119.89695 |
| Thadp | hb–bt | JHCP-68 | 60.79 | 0.67 | 18.44 | 5.25 | 0.06 | 2.16 | 6.08 | 4.4 | 1.88 | 1.8 | 0.287 | 100.02 | Andesite | 38.66332 | 119.89796 |
| Thadp | hb–bt | JHCP-69 | 58.73 | 0.74 | 18.91 | 6.19 | 0.07 | 2.22 | 6.69 | 4.16 | 1.9 | – | 0.29 | 99.90 | Andesite | 38.66440 | 119.89472 |
| Taa | hb–bt | JHCP-34 | 60.75 | 0.71 | 17.68 | 6.11 | 0.08 | 3.27 | 5.68 | 3.65 | 1.91 | 19.7 | 0.285 | 100.13 | Andesite | 38.63979 | 119.93361 |
| Taa | hb–bt | JHCP-55 | 68.48 | 0.37 | 17.09 | 4.09 | 0.06 | 0.55 | 3.04 | 3.74 | 2.3 | – | 0.242 | 99.96 | Dacite | 38.66626 | 119.96749 |
| Taa | hb–bt | JHCP-27 | 64.26 | 0.41 | 18.14 | 4.27 | 0.12 | 1.26 | 4.59 | 4.33 | 2.35 | – | 0.267 | 100.00 | Dacite | 38.66667 | 119.96321 |
| Taa | hb–bt | JHCP-84 | 61.07 | 0.79 | 19.04 | 6.35 | 0.03 | 2.3 | 4.19 | 4 | 1.79 | – | 0.204 | 99.77 | Andesite | 38.66578 | 119.97672 |
| Taa | hb–bt | JHCP-49 | 60.51 | 1 | 16.65 | 6.97 | 0.09 | 2.83 | 6.21 | 3.17 | 2.57 | 4.3 | 0.508 | 100.51 | Andesite | 38.63720 | 119.92142 |
| Tri | hb–bt | JHCP-38 | 72.7 | 0.21 | 15.85 | 1.75 | 0.08 | 0.26 | 2.62 | 3.5 | 2.49 | – | 0.105 | 99.57 | Rhyolite | 38.66458 | 119.95439 |
| Thaba1 | hb–bt | SBDCP46 | 58.43 | 0.85 | 17.05 | 6.04 | 0.05 | 3.08 | 6.02 | 3.88 | 2.56 | 29.6 | 0.433 | 98.40 | Trachyandesite | 38.70489 | 119.99347 |
| Tfdf** | hb–bt | SBDCP67 | 55.98 | 1.06 | 17.75 | 7.36 | 0.05 | 3.85 | 8.05 | 3.68 | 1.98 | 0 | 0.248 | 100.01 | Basaltic andesite | 38.70703 | 120.10581 |

Data organized by phenocrystic content. All map units analysed are shown chronostratigraphically in Figure 2(b). Samples labelled 'JHCP' are plotted on the geologic map in Figure 2(a). Chemistry of samples labelled ** and 'SBD' was reported in the data repository of Busby *et al.* (2008a); modal analyses and plots of the samples on a geologic map were presented in that paper. Rock names are from Figure 6. [1]Geochemistry on clast within labelled debris-flow deposit. [2]Geochemistry on small-volume block-and-ash-flow tuff within labelled debris-flow deposit. [3]Geochemistry on small dike within labelled debris-flow deposit.

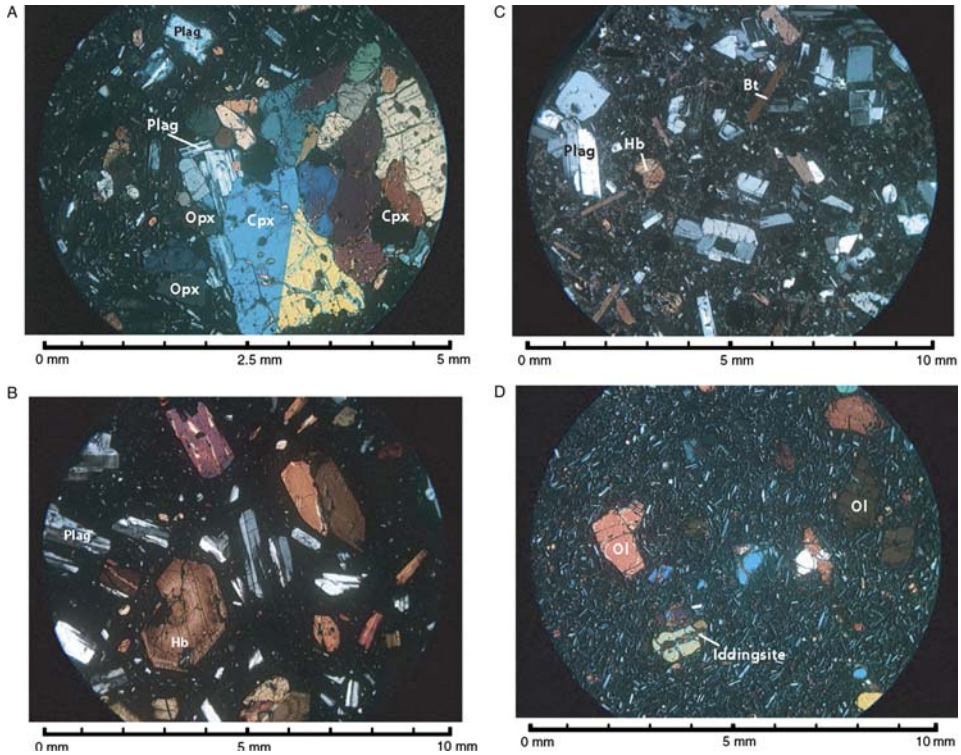


Figure 7. Photomicrographs of selected rocks dated in this study, showing that these Miocene rocks have unaltered plagioclase, clinopyroxene, orthopyroxene, hornblende, and biotite. (a) Photomicrograph of the western sequence 3 10.70 ± 0.1 Ma Pickett Peak two pyroxene andesite intrusions (Tpai; Figure 2) in crossed polarized light. Cluster of large clinopyroxene (cpx) surrounded by plagioclase (plag) and orthopyroxene (opx). (b) Photomicrograph of the upper hornblende andesite lava flow (Thalu; Figure 2) dated at 6.18 ± 0.14 Ma in crossed polarized light. Note the zoning of the hornblende (hb), with its distinctive cleavage angles and the euhedral plagioclase crystals (plag). (c) Photomicrograph of the Markleeville Peak hornblende–biotite andesite and dacite intrusion (Thbdi; Figure 2) in crossed polarized light, containing both biotite (bt) and hornblende (hb). (d) Photomicrograph of an olivine basaltic intrusion (Tbi) where the olivine (Ol) has begun to alter to iddingsite in a fine-grained plagioclase plus olivine groundmass. Intrusion cut fluvial deposits on the Sierran crest (sample 20).

fluvial deposits (Tvf1) and the lower hornblende andesite flow is visible in aerial photographs and in the field. The lower hornblende andesite lava flow has a basal breccia of varying thickness, averaging 4 m, with sparse accidental clasts, passing upwards into a coherent interior ~60 m (200 ft) thick and containing hornblende crystals up to 0.4 cm long, with columnar jointing. A prominent bench marks the top of the hornblende andesite flow at its northern extent. A hornblende andesite block-and-ash-flow tuff forms lenses that are too thin to map between the lower and upper flows on the north margin of their exposure, but thickens southwards, at the expense of the lower flow, where it is mapped as a separate unit (Thaba3; Figure 2). This block-and-ash-flow tuff is described below.

The upper lava flow (Thalu) is a crystal-rich porphyritic hornblende andesite, with hornblende phenocrysts up to 1 cm long (Figure 7(b)). The basal breccia is ~10 m (~30 ft) thick with an irregular base (Figure 4(b)). There is no evidence for a preserved flow-top breccia and it is locally overlain by a debris-flow deposit (Figure 2(a)), although

Table 3. Summary of the $^{40}Ar/^{39}Ar$ dates we have acquired for the Hope Valley–Carson Pass–Kirkwood region.

| Sample | Map unit | Geochem | Mineral dated | Lat (°N) | Long (°W) | Nominal age (Ma)[1] | | Preferred age (Ma)[2] | | Unit name |
|---|---|---|---|---|---|---|---|---|---|---|
| | | | | | | Age | ± 2σ | Age | ± 2σ | |
| **Sequence 2** | | | | | | | | | | |
| JHCP-7 | Tphaba | Andesite | Plagioclase | 38.6433 | 119.9037 | 15.4 | 0.6 | 15.5 | 0.6 | Jeff Davis Peak pyx-hb andesite and dacite block-and-ash-flow tuff |
| SBDCP30 | Thaba1 | Trachyandesite | Biotite | 38.7014 | 120.0003 | 14.91 | 0.06 | 15.01 | 0.06 | Carson Pass hornblende trachyandesite block-and-ash-flow tuff (recalculated from Busby *et al.* 2008a) |
| JHCP-14 | Thaba2 | Andesite | Hornblende | 38.7184 | 119.9853 | 13.51 | 0.16 | 13.61 | 0.16 | Red Lake Peak hb andesite block-and-ash-flow tuff |
| **Sequence 3** | | | | | | | | | | |
| JHCP-44 | Tpai | Andesite | Hornblende | 38.7544 | 119.8969 | 10.70 | 0.10 | 10.77 | 0.10 | Pyroxene andesite intrusion of Pickett Peak |
| **Sequence 4** | | | | | | | | | | |
| SBDCP62 | Tbl | Basalt | Whole rock | 38.7101 | 120.0187 | 6.90 | 0.20 | 6.95 | 0.20 | Basalt lava flow (recalculated from Busby *et al.* 2008a) |
| JHCP-69 | Thadp | Andesite | Hornblende | 38.6644 | 119.8947 | 6.33 | 0.24 | 6.37 | 0.24 | Hornblende andesite dike of Markleeville Peak |
| JHCP-53 | Thbdi | Dacite | Hornblende | 38.6581 | 119.9233 | 6.30 | 0.14 | 6.34 | 0.14 | Markleeville Peak hb-bt dacite and andesite intrusions |
| JHCP-67 | Thbdi | Andesite | Hornblende | 38.6600 | 119.8996 | 6.14 | 0.14 | 6.18 | 0.14 | Markleeville Peak hb-bt dacite and andesite intrusions |
| JHCP-13 | Tpaba | Basaltic andesite | Hornblende | 38.7122 | 119.9856 | 6.25 | 0.10 | 6.29 | 0.10 | Red Lake Peak pyroxene basaltic andesite block-and-ash-flow tuff |
| ERLPk | Tpaba | NA | Hornblende | 38.7158 | 119.9857 | 6.09 | 0.34 | 6.13 | 0.34 | Red Lake Peak pyroxene basaltic andesite block-and-ash-flow tuff |
| JHCP-56 | Thalu | Andesite | Hornblende | 38.6909 | 119.9799 | 6.18 | 0.14 | 6.22 | 0.14 | Lower hornblende andesite lava flow |

Locations for samples are plotted in Figure 2(a). This table includes the two dates for map units Tbl and Thaba1 that were previously presented in Busby *et al.* (2008a). Map unit Thaba1 was previously labelled Taba1 in Figure 2 of Busby *et al.* (2008a).

[1]Nominal age is calculated using 28.02 Ma for the FCs standard (Renne *et al.* 1998).

[2]Preferred age is calculated using 28.201 Ma for the FCs standard (Kuiper *et al.* 2008).

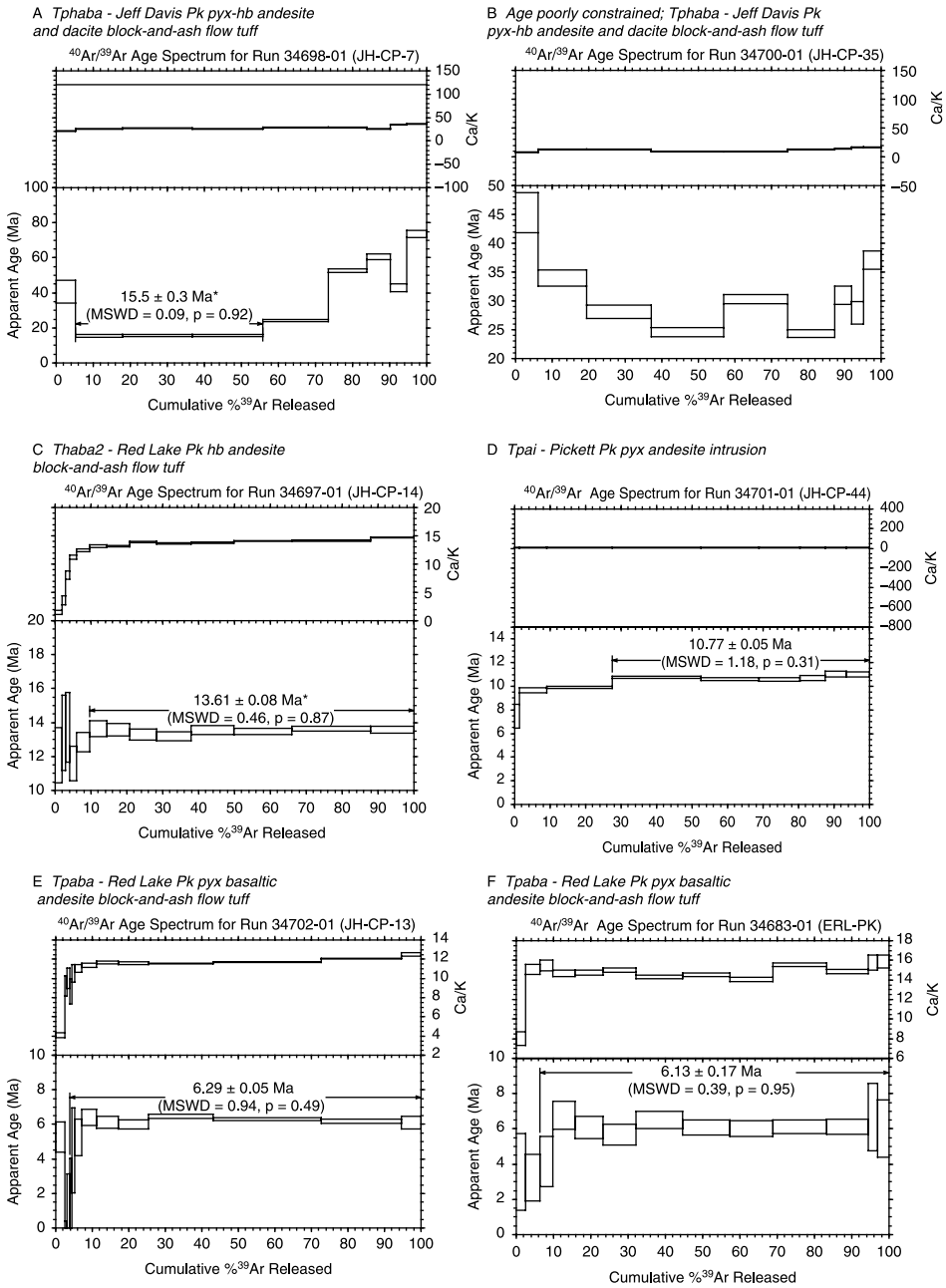
A Tphaba - Jeff Davis Pk pyx-hb andesite and dacite block-and-ash flow tuff
40Ar/39Ar Age Spectrum for Run 34698-01 (JH-CP-7)
15.5 ± 0.3 Ma*
(MSWD = 0.09, p = 0.92)
Apparent Age (Ma)
Ca/K
Cumulative %39Ar Released
B Age poorly constrained; Tphaba - Jeff Davis Pk pyx-hb andesite and dacite block-and-ash flow tuff
40Ar/39Ar Age Spectrum for Run 34700-01 (JH-CP-35)
Apparent Age (Ma)
Ca/K
Cumulative %39Ar Released
C Thaba2 - Red Lake Pk hb andesite block-and-ash flow tuff
40Ar/39Ar Age Spectrum for Run 34697-01 (JH-CP-14)
13.61 ± 0.08 Ma*
(MSWD = 0.46, p = 0.87)
Apparent Age (Ma)
Ca/K
Cumulative %39Ar Released
D Tpai - Pickett Pk pyx andesite intrusion
40Ar/39Ar Age Spectrum for Run 34701-01 (JH-CP-44)
10.77 ± 0.05 Ma
(MSWD = 1.18, p = 0.31)
Apparent Age (Ma)
Ca/K
Cumulative %39Ar Released
E Tpaba - Red Lake Pk pyx basaltic andesite block-and-ash flow tuff
40Ar/39Ar Age Spectrum for Run 34702-01 (JH-CP-13)
6.29 ± 0.05 Ma
(MSWD = 0.94, p = 0.49)
Apparent Age (Ma)
Ca/K
Cumulative %39Ar Released
F Tpaba - Red Lake Pk pyx basaltic andesite block-and-ash flow tuff
40Ar/39Ar Age Spectrum for Run 34683-01 (ERL-PK)
6.13 ± 0.17 Ma
(MSWD = 0.39, p = 0.95)
Apparent Age (Ma)
Ca/K
Cumulative %39Ar Released

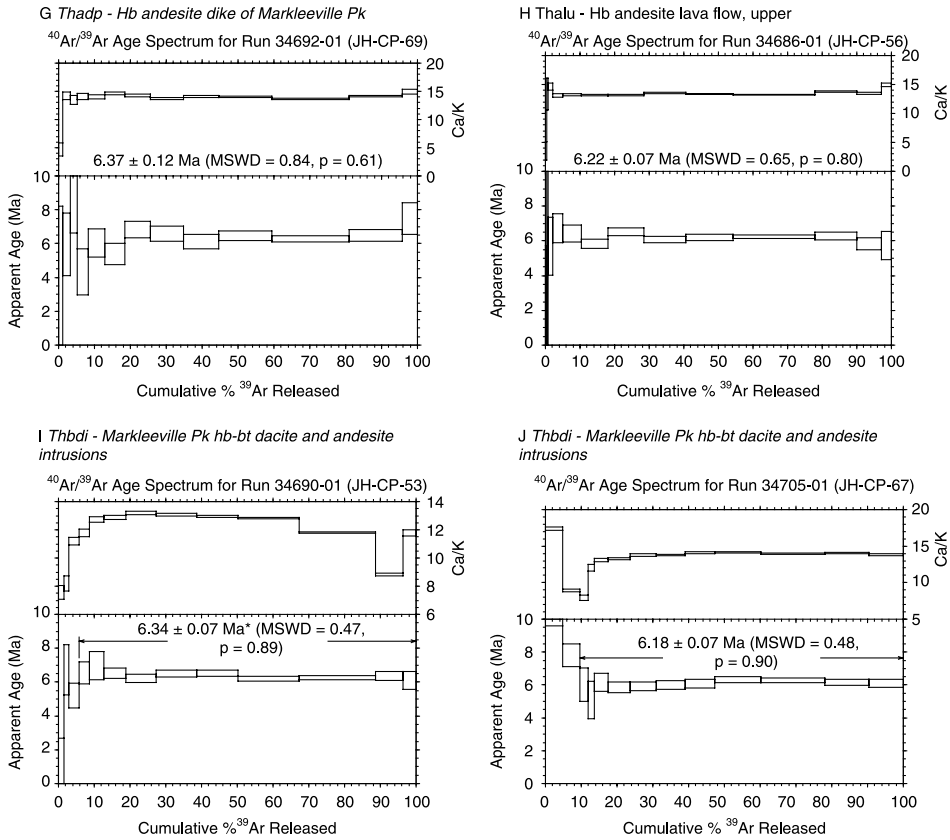


Figure 8. $^{40}Ar/^{39}Ar$ age spectra for samples from Hope Valley. See Figure 2 for sample localities, Table 2 for a summary of the data, and Table 3 for GPS localities. Plateau ages are shown with errors at one standard deviation. (a) Plagioclase age spectrum for the Jeff Davis Peak pyroxene–hornblende andesite and dacite block-and-ash-flow tuff (Tphaba), sequence 2. (b) Plagioclase age spectrum for the Jeff Davis Peak pyroxene–hornblende andesite and dacite block-and-ash-flow tuff (Tphaba), sequence 2. (c) Hornblende age spectrum for the Red Lake Peak hornblende andesite block-and-ash-flow tuff (Thaba2), sequence 2. (d) Hornblende age spectrum for the Pickett Peak pyroxene andesite intrusion (Tpai), sequence 3. (e) Hornblende age spectrum for the Red Lake Peak pyroxene basaltic andesite block-and-ash-flow tuff (Tpaba), sequence 4. (f) Hornblende age spectrum for the Red Lake Peak pyroxene basaltic andesite block-and-ash-flow tuff (Tpaba), sequence 4. (g) Hornblende age spectrum for the Markleeville Peak hornblende andesite dike (Thadp), sequence 4. (h) Hornblende age spectrum for the upper hornblende andesite lava flow (Thalu), sequence 4. (i) Hornblende age spectrum for the Markleeville Peak hornblende–biotite dacite and andesite intrusions (Thbdi), sequence 4. (j) Hornblende age spectrum for the Markleeville Peak hornblende–biotite dacite and andesite intrusions (Thbdi), sequence 4.

the flow top does form a slight bench in the topography. The upper flow is less extensive and thicker (>100 m thick) than the lower flow (Thall). The upper flow yielded a hornblende $^{40}Ar/^{39}Ar$ date of 6.22 ± 0.14 Ma (Figure 8(h); Table 2). We tentatively infer that two lava flows were erupted from the Red Lake Fault, because they lie along it and are restricted to the hanging wall of the fault (see Hope Valley Graben, below).

To summarize, lava flows in the Carson Pass–Markleeville region are small volume and include one section of olivine basalt flows and one section consisting of two

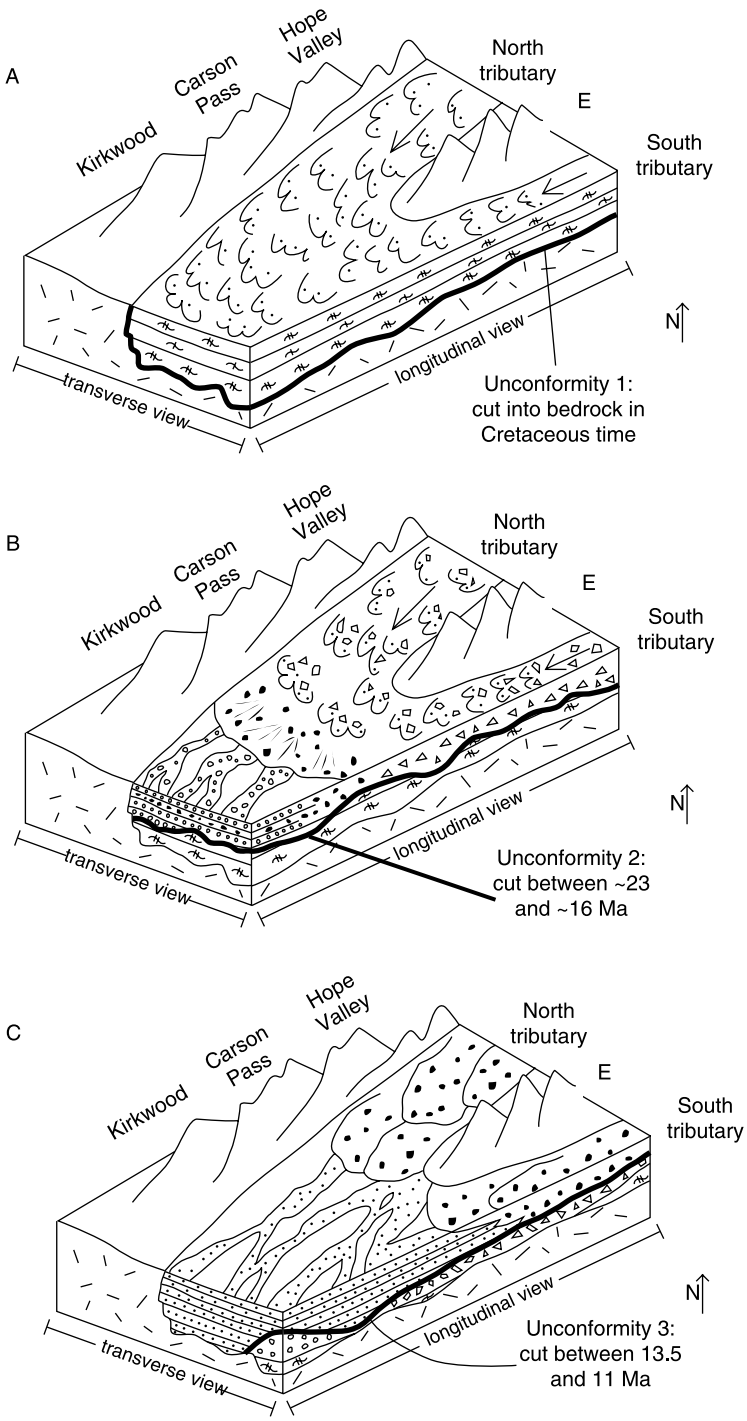
A
Kirkwood
Carson Pass
Hope Valley
North tributary
E
South tributary
N
transverse view
longitudinal view
Unconformity 1: cut into bedrock in Cretaceous time
B
Kirkwood
Carson Pass
Hope Valley
North tributary
E
South tributary
N
transverse view
longitudinal view
Unconformity 2: cut between ~23 and ~16 Ma
C
Kirkwood
Carson Pass
Hope Valley
North tributary
E
South tributary
N
transverse view
longitudinal view
Unconformity 3: cut between 13.5 and 11 Ma

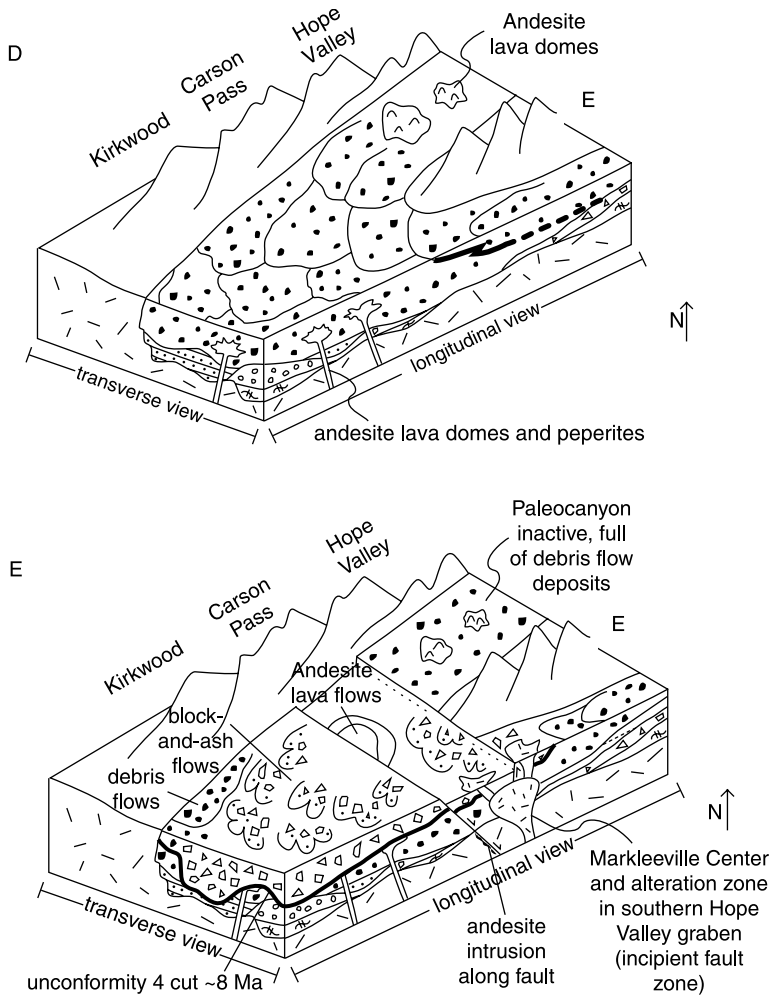


Figure 9. A block diagram of the Hope Valley–Carson Pass–Kirkwood Valley area, modelling the topographic and volcaniclastic evolution from Oligocene until late Miocene. Volcanic debris was transported down the palaeotributaries in the east (upper right), and merged to form one palaeocanyon in the west (lower left). (a) Unconformity 1, the contact between granitic basement rock and Tertiary volcanic rock, was cut into the bedrock in the Cretaceous. From 30 to 23 Ma, the Oligocene ignimbrites filled the palaeocanyon. (b) Unconformity surface 2 formed between ~23 and ~16 Ma, and eroded away much of the ignimbrite deposits. Then, from 16 to ~13.5 Ma, the palaeocanyons filled with block-and-ash-flow tuffs (Tphaba, Thaba1, and Thaba2), which were reworked down-canyon into debris-flow and fluvial deposits (Figure 2; Busby *et al.* 2008a). (c) Unconformity 3 was cut between 13.5 and 11 Ma, after the block-and-ash-flow tuff deposition (Thaba2) and before the deposition of thick fluvial deposits fed by debris-flow lobes (Tvf1). (d) Unconformities 4 and 5 are mapped in the Kirkwood region (Busby *et al.* 2008a), but are not found within the massive debris-flow deposits of Hope Valley (Tvdf1). They may not exist, or may be cryptic and not visible due to the lack of bedding. At 10.7 Ma, lava domes, volcanic necks (Tpai), and peperites intruded into the debris-flow deposits (Busby *et al.* 2008a). (e) Unconformity 4 was cut post 10.5 Ma, but prior to 6.9 Ma. Volcanic activity resumed at 6.9 Ma (Tbl) and continued through ~6 Ma (Thbdi and Tpaba) or possibly 5.2 Ma (Thai; Armin *et al.* 1984). The Red Lake and Hope Valley faults were active by 6 Ma, as shown by eruption of the hornblende andesite lava flows through the former, and emplacement of the Markleeville intrusive complex along the latter.

hornblende andesite flows with intervening block-and-ash-flow tuff. They are restricted to the youngest sequence (4), at about 6 Ma.

### *Block-and-ash-flow tuffs*

Block-and-ash-flow tuffs are the most common primary volcanic rock type in the area. The block-and-ash-flow tuffs are small-volume pyroclastic-flow deposits characterized by a large fraction of monolithic juvenile blocks set in a massive, unsorted, medium- to coarse-grained ash matrix of the same composition (Figure 4(c)). They commonly show evidence for hot emplacement, such as bread-crust texture on blocks (Figure 4(d)), jigsaw-fit texture indicating *in situ* fragmentation, and carbonized wood. These textures cannot survive significant transport, and indicate vent-proximal locations (Fisher and Schminke 1984; Miyabuchi 1999; Freundt *et al.* 2000). The block-and-ash-flow tuffs also show evidence for hot emplacement with oxidized bases and tops of flows (unit Tpaba; Figure 4(e)). Explosive volcanic deposits, such as ash fall or pumiceous fall or flow deposits, are absent from Miocene rocks in the map area and the central Sierra in general; thus, the block-and-ash-flow tuffs probably formed by lava dome collapse (Fisher and Heiken 1982; Camus *et al.* 2000; Voight *et al.* 2000).

The oldest block-and-ash-flow tuff (Tphaba of sequence 2; Table 1) is also the most extensively preserved block-and-ash-flow tuff in the field area. It lies on the east side of the Hope Valley Graben, in the southeast tributary south of Markleeville Peak, and forms a unit up to 195 m (640 ft) thick. Its blocks are relatively small (dominantly lapilli-sized), and it has minor debris-flow deposits interstratified with it, suggesting that it represents medial rather than proximal facies of lava dome collapse. This block-and-ash-flow tuff contains a phenocryst assemblage of two pyroxenes, hornblende, and plagioclase (Figure 5). Plagioclase from two samples of this unit reveals saddle-shaped age spectra indicative of excess Ar (Figure 8(a,b)); the saddle minimum age of 15.5 ± 0.6 Ma (Figure 8(a)) is interpreted to be a maximum age for this unit.

The second oldest block-and-ash-flow tuff (Thaba1 of sequence 2; Figure 2; Table 1) is only slightly younger than the oldest; it was dated by Busby *et al.* (2008a) at 14.69 ± 0.06 Ma and recalculated to our preferred age of 15.5 ± 0.06 Ma. This grey-coloured unit lies west of the Hope Valley Graben along the present-day Sierra Nevada crest (Figure 2), and is preserved as a 210 m (700 ft) thick erosional remnant at the base of the main palaeocanyon (see Figure 4(b) of Busby *et al.* 2008a), where the two palaeotributaries apparently joined (Figure 1(b)). This hornblende trachyandesite block-and-ash-flow tuff contains abundant large blocks, as well as complexly intercalated debris-flow deposits, suggesting mixing of primary and reworked deposits by slumping (Busby *et al.* 2008a).

The third oldest block-and-ash-flow tuff (Thaba2 of sequence 2; Figure 2; Table 1) is a white orthopyroxene–biotite–hornblende block-and-ash-flow tuff that was at least 90 m (300 ft) thick. It has a hornblende $^{40}Ar/^{39}Ar$ date of 13.61 ± 0.16 Ma (Figure 8(c)). This unit is only preserved at the base of the palaeocanyon at the Sierran crest, where it directly overlies basement metamorphic rocks (Figure 2).

Both of these block-and-ash-flow tuffs (Thaba1 and Thaba2) underlie the fluvial deposits of unit Tvf1, and were deeply incised by the palaeoriver. Erosional remnants remained on the walls of the palaeocanyon, even though the younger fluvial deposits (Tvf1) fill lower elevations to their northwest (Figure 2(a)).

In the southwestern part of the map area, we mapped a block-and-ash-flow tuff (Thaba3 of sequence 4; Figure 2; Table 1) between the two lava flows (Thall and Thalu).

This unit is a hornblende andesite of similar mineralogy and geochemistry to the lava flows (Figures 5 and 6). It is thickest at the south end of the flows, where it is up to 95 m (320 ft), and lenses out to the north. Because it is interstratified with the lava flows, it must be 6.22 ± 0.14 Ma or slightly older (Table 3).

A two-pyroxene andesite block-and-ash-flow tuff (Tpaba of sequence 4; Figure 2; Table 1) overlies sequence 4 debris-flow deposits (Tvdf2), as well as sequence 2 block-and-ash-flow tuffs (Thaba2), forming Red Lake Peak (Figures 2(a) and 4(e)). It is about 65 m (220 ft) thick, although much of it has likely been eroded. Two samples from this unit have $^{40}Ar/^{39}Ar$ ages of 6.29 ± 0.10 and 6.13 ± 0.34 Ma (Figure 8(e,f)). These ages are the same as that on the Sentinels two-pyroxene andesite block-and-ash-flow tuff in Kirkwood Valley (6.18 ± 0.12 Ma; Table 4; recalculated from Busby *et al.* 2008a; unit Taba3 of Figure 2(a)).

### *Debris-flow deposits*

Volcanic debris-flow deposits (map units Tvdf1 and Tvdf2; Table 1) are massive to thick-bedded matrix-supported deposits with sub-rounded to angular clasts that range in size from pebble to boulder (up to 15 m in diameter); they are unsorted and show no internal stratification. The abundance of the matrix varies and is commonly coarse-grained volcanic lithic sandstone. Debris-flow deposits are polylithic, but nearly all of the clasts are some variety of andesitic rock, with minor mafic volcanic rock fragments, granitic rock fragments, and sparse silicified or petrified wood fragments (Figure 4(f)). Unlike block-and-ash-flow tuffs, debris-flow deposits do not contain blocks with bread-crust texture or prismatically jointed blocks. They can also be distinguished by their tan, rather than grey, colour. Although the debris-flow deposits in the map area are indistinguishable from one another in outcrop, they are divided by their stratigraphic position relative to other map units. They frequently contain minor lenses of fluvial conglomerates, sandstones, and flood-flow deposits, but these are too small to map, and have been grouped into the debris-flow deposit units (Figure 4(g)). First, the older debris-flow map unit (Tvdf1 of sequence 3) is described, and then the younger debris-flow map unit (Tvdf2 of sequence 4; Figure 2(b)) is described.

In the southeastern palaeotributary (Figure 1(b)), at Jeff Davis Peak, we mapped a debris-flow deposit (Tvdf1 of sequence 3) that rests upon the oldest block-and-ash-flow tuff in the map area (Tphaba of sequence 2; Figure 2(a)). It measures 175 m (580 ft) thick. This map unit is dominated by debris-flow deposits, but also contains minor flood-flow and fluvial deposits of well-stratified coarse-grained sandstone and clast-supported conglomerate. Block size in the debris-flow deposits increases upsection to 2 m. The top of the section on Jeff Davis Peak has crude stratification dipping 20° north, and contains a lens of block-and-ash-flow tuff. The steepness of this dip indicates that it is probably a slide block within the debris-flow deposit. We correlate this debris-flow deposit (Tvdf1) across the Markleeville Peak intrusive complex to debris-flow deposits on both sides of Charity Valley (Figure 2). These deposits are up to 210 m (700 ft) thick and were deposited directly on granitic basement, suggesting that they onlap the north wall of the southeastern palaeotributary.

In the northeastern palaeocanyon tributary, on the east side of Hope Valley (Figure 2(a)), the older volcanic debris-flow map unit (Tvdf1 of sequence 3; Table 1) forms nearly all of the Pickett Peak and Hawkins Peak areas. These debris-flow deposits have a cliff-forming clast-supported base of flood-flow deposits that grades upwards into a more matrix-rich deposit. Crude bedding strikes N–S and dips 4° west. The preserved

Table 4. Summary of the recalculated $^{40}Ar/^{39}Ar$ dates from Busby *et al.* (2008a).

| Sample | Map unit | Geochem | Mineral dated | Lat (°N) | Long (°W) | Original age (Ma)[1] | | Nominal age (Ma)[2] | | Preferred age (Ma)[3] | | Unit name |
|---|---|---|---|---|---|---|---|---|---|---|---|---|
| | | | | | | Age | ±2σ | Age | ±2σ | Age | ±2σ | |
| SBDCP29 | Trt | – | Single sanidine | 38.70768 | 120.02590 | 22.9 | 0.1 | 23.2 | 0.1 | 23.4 | 0.1 | Reworked pumice lapilli tuff |
| SBDCP29 | Trt | – | Single sanidine | 38.70768 | 120.02590 | 23.2 | 0.1 | 23.6 | 0.1 | 23.7 | 0.1 | ″ |
| SBDCP29 | Trt | – | Fusion of several grains | 38.70768 | 120.02590 | 23.4 | 0.1 | 23.4 | 0.1 | 23.9 | 0.1 | ″ |
| SBDCP30 | Taba1 | Trachy-andesite | Biotite | 38.70140 | 120.00030 | 14.69 | 0.06 | 14.91 | 0.06 | 15.01 | 0.06 | Trachyandesite block-and-ash-flow tuff of Carson Pass |
| SBDCP30 | Taba1 | ″ | Plagioclase | 38.70140 | 120.00030 | 14.1 | 0.7 | 14.3 | 0.7 | 14.4 | 0.7 | ″ |
| SBDCP20 | Tvdf1 | – | Plagioclase | 38.68548 | 120.06170 | 10.49 | 0.12 | 10.65 | 0.12 | 10.72 | 0.12 | Peperite dike in volcanic debris-flow deposits of Kirkwood Valley |
| SBDCP62 | Tbl | Basalt | Whole rock | 38.71008 | 120.01867 | 6.80 | 0.20 | 6.90 | 0.20 | 6.95 | 0.20 | Basalt lava flows of Carson Pass |
| SBDCP61 | Taba3 | Andesite | Plagioclase | 38.69210 | 120.08658 | 6.05 | 0.12 | 6.14 | 0.12 | 6.18 | 0.12 | Andesite block-and-ash-flow tuff of the Sentinels |

[1]Original age is calculated using 27.60 Ma for the FCs standard as reported by Gans (Busby *et al.* 2008b).
[2]Nominal age is calculated using 28.02 Ma for the FCs standard (Renne *et al.* 1998).
[3]Preferred age is calculated using 28.201 Ma for the FCs standard (Kuiper *et al.* 2008).

thickness of the deposit is at least 450 m (1500 ft), and an additional 60 m (200 ft) must have eroded away to expose the intrusions that make up Pickett Peak and Hawkins Peak. We correlate these debris-flow deposits (Tvdf1) with those that lie to the northeast, across the modern west fork of the Carson River, where debris-flow deposits of Horsethief Mountain (Tvdf1; Figure 2(a)) are more than 490 m (1600 ft) thick, and rise 135 m (445 ft) above the surrounding granite. The basal contact is gradational with underlying fluvial deposits (Tvf1). Similar to the deposits to the south at Pickett Peak, this unit grades upwards from clast-supported flood-flow deposits to matrix-supported debris-flow deposits.

The younger debris-flow deposit map unit (Tvdf2 of sequence 4; Table 1) is preserved in the western part of the Hope Valley graben and along the present-day Sierran crest (Figure 2), in the region where the two palaeotributaries merge to form a single palaeocanyon (Figure 1(b)). Within the graben, east of Elephant's Back, a debris-flow deposit (Tvdf2) rests upon both the upper and lower andesitic lava flows (Thall and Thalu; Figure 2(a)). In some localities, the base of the debris-flow deposit interfingers with the block-and-ash-flow tuff (Thaba3) that lies between the two lava flows (Figure 4(d)). The upper part of the deposit contains a 30 m long clast of flow-banded andesite that is geochemically similar to the 10.77 ± 0.1 Ma Pickett Peak and Hawkins Peak intrusions (Tpai; sample 65; Figure 6). The deposit measures 115 m (380 ft) thick in both localities. Where the debris-flow deposits rest directly on the lower andesite lava flow, the lava flow's flow-top breccia is preserved beneath it. Since there is no evidence for a debris flow between the two flows, we infer that deposition of the debris flow post-dated emplacement of both the lava flows and filled palaeotopography created by emplacement of the second flow. Therefore, the younger debris-flow deposit (Tvdf2) is younger than the upper andesite lava flow (Thalu), which is 6.22 ± 0.14 Ma (Table 3).

The younger debris-flow deposit (Tvdf2) also crops out on the Sierran crest west of the Hope Valley graben, in the footwall of the Red Lake Fault (Figure 2), where it is at least 160 m (520 ft) thick. It overlies fluvial deposits, and has a readily identifiable contact defined by the change in slope: the fluvial deposits are cliff-formers, while the debris-flow deposits are slope-formers. There, the 200 m (660 ft) thick deposit overlies 6.95 ± 0.20 Ma basalt lava flows (Tbl; Figure 2; Table 3), and is overlain by the Red Lake Peak pyroxene andesite block-and-ash-flow tuff (Tpaba) at 6.13 ± 0.34 to 6.29 ± 0.10 Ma (Figure 8(e,f); Table 3).

### *Fluvial deposits*

Fluvial deposits in the Carson Pass area are highly varied, but commonly are poor- to well-stratified, well-sorted, clast-supported conglomerates composed primarily of sub-rounded to rounded andesitic volcanic clasts (Figure 4(h)). Clasts range in size from pebble to boulders (up to 1 m in diameter). Sandstone beds are planar-laminated and cross-laminated, with cut-and-fill structures. A fluvial sandstone unit is present at the base of sequence 2, which contains only minor pebble conglomerate (Tvs), and two fluvial conglomerate units contain lesser sandstone interbeds (Tvf1 and Tvf2 of sequence 3; Figure 2).

We correlate the volcanic fluvial sandstone unit (Tvs of sequence 2; Figure 2(b)) from the footwall of the Red Lake Fault, east into the Hope Valley graben, and farther east into the footwall of the Hope Valley Fault, in the northeastern palaeotributary at Horsethief Canyon and in the southeastern palaeotributary at Jeff Davis Peak. This unit thus forms the basal unit of the Miocene section. In the footwall of the Red Lake Fault at Elephant's

Back, the volcanic fluvial sandstone (Tvs) consists of a well-sorted, sub-rounded, coarse-grained volcaniclastic sandstone with thin interbeds of siltstone (Tvs), which grades upwards into a stratified cobble conglomerate-breccia (Tsb; Figure 2; Table 1). The conglomerate-breccia is clast-supported, medium-bedded with a sandstone matrix, and is altered to a distinctive purplish-grey colour. The same conglomerate-breccia (Tsb) is dropped down to the east into the Hope Valley graben along the Red Lake Fault, as discussed below. The volcanic fluvial sandstone (Tvs) at Horsethief Canyon and the northwest end of the Sierran crest has pebble-sized clasts of pumice and sanidine-bearing silicic ignimbrite fragments derived from the Oligocene ignimbrites (Ti). The volcanic fluvial sandstone (Tvs) at Jeff Davis Peak is a well-sorted, coarse-grained sandstone, with andesite fragments and crystals of plagioclase, hornblende, and pyroxene. It was presumably deposited on top of the Valley Springs Formation in the southeastern palaeotributary, but the contact relations have been obliterated by the Markleeville Peak intrusions (Thbdi). It is overlain in erosional unconformity by the 15.5 ± 0.6 Ma Jeff Davis Peak pyroxene–hornblende andesite block-and-ash-flow tuff (Tphaba; Figure 2).

The lower of the two fluvial conglomerate and sandstone units (Tvf1 of sequence 3; Figure 2; Table 1) is the most extensive map unit in the Hope Valley–Carson Pass–Kirkwood palaeocanyon. It occurs east of the Hope Valley graben at Horsethief Canyon (in the northeastern palaeotributary), it lies within the graben south of Red Lake, and it forms much of the Sierra crest north of Carson Pass (Figure 2). From there, we have mapped it another 12 km westwards in the Carson Pass–Kirkwood palaeocanyon, where it forms a section up to 300 m thick (Busby *et al.* 2008a). At the Sierran crest, the fluvial conglomerate and sandstone unit (Tvf1) is 300 m (1000 ft) thick, and up to 275 m (900 ft) of it lies in buttress unconformity against sequence 2 block-and-ash-flow tuffs and basement rocks. Bedding dips 6°–9° to the west, with cut-and-fill structures and trough cross-laminations that give a palaeocurrent direction of flow to the south/southwest. It is sandier near the base and becomes more conglomeratic towards the top, where much of the section is cliff-forming. At Horsethief Canyon, the fluvial conglomerate and sandstone unit (Tvf1) is greater than 275 m (900 ft) thick and dips ~10° west. The age of the fluvial conglomerate and sandstone unit was stratigraphically constrained between 15.01 ± 0.06 and 10.72 ± 0.12 Ma by Busby *et al.* (2008a; recalculated dates shown in Table 4). Our new dates further constrain the age of this unit to be between 13.61 ± 0.16 and 10.72 ± 0.12 Ma, i.e. after deposition of the Red Lake Peak hornblende andesite block-and-ash-flow tuff (Thaba2; Table 3) and before the intrusion of a peperitic andesite dike in debris-flow deposits that overlie it (Tvdf1) in Kirkwood Valley (Table 4; Busby *et al.* 2008a).

The upper of the two fluvial conglomerate and sandstone units (Tvf2 of sequence 3; Figure 2; Table 1) is restricted to the southeastern palaeotributary north of Charity Valley (Figure 2) and is at most 50 m (160 ft) thick; it is distinguished from the lower fluvial conglomerate and sandstone unit (Tvf1) by its stratigraphic position above, rather than below, the lower debris-flow unit (Tvdf1).

### *Altered andesite*

Altered andesitic volcanic rocks (Taa) lie within the southern end of the Hope Valley graben (Taa; Figure 2; Table 1). These are block-and-ash-flow tuffs, lava flows, intrusions, and debris-flow deposits that are too strongly altered to map individually. The altered rocks are hornblende and plagioclase phyric andesites (samples 27 and 34; Figures 5 and 6), with plagioclase largely altered to clay, hornblende either completely oxidized or with oxidized

rims, and epidote common. The rocks are purple to red to copper-tinged green due to propylitic alteration. This unit is intruded by small, irregularly shaped hornblende–biotite dacites (Thbdi and Thadp), similar to the much larger intrusive complex and hornblende andesite dikes and plugs that make up Markleeville Peak on the footwall of the Hope Valley Fault to the east (Figure 2(a)). As discussed below, we interpret the altered andesite unit (Taa) to represent the altered roof rocks of the Markleeville Peak intrusive complex, which have been down-dropped into the Hope Valley graben. Furthermore, we interpret the small, irregular hornblende–biotite dacite to represent apophyses coming off the top of the Markleeville Peak intrusions. The altered andesite unit is also intruded by a small altered rhyolite plug of unknown age (Tri; Figure 2; Table 1). It has Liesegang banding and is too altered to be suitable for modal analysis.

## Sequence statigraphy

In this section, we reconstruct the stratigraphic evolution of the Hope Valley–Carson Pass–Kirkwood palaeocanyon system in a series of time slices, by describing each unconformity and the strata that lie above it. The basal unconformity (unconformity 1), where Cenozoic strata fill a palaeocanyon cut into Cretaceous mesozonal granitic rock, is by far the most obvious unconformity. As noted above, the shape of the contact between basement rocks and Cenozoic cover defines two palaeotributaries that merge at the present-day Sierran crest (Figure 1(b)).

Unconformity surfaces within the palaeocanyon fill are more easily mapped from the Sierran crest westwards to the Kirkwood Valley area (Busby *et al.* 2008a) than they are east of the crest in the Hope Valley area (Figure 2). This is because the rocks are unfaulted from the crest westwards, exposures are better there, and intrusions and associated altered rocks are less abundant there. Nonetheless, we have been able to map and correlate most of the unconformity surfaces, described by Busby *et al.* (2008a) for the Carson Pass–Kirkwood segment, into the Hope Valley segment of the palaeocanyon. Only unconformity surfaces 4 and 5 could not be traced into Hope Valley, but these have limited lateral extent in Kirkwood Valley and are not interpreted to record significant tectonic events (Busby *et al.* 2008a,b). Unconformities 1–3, and 6 are not only traceable along the length of the Hope Valley–Carson Pass–Kirkwood palaeocanyon, but are also age-correlative with the deepest, most extensive unconformities in other parts of the central Sierra (Busby *et al.* 2008b; Busby and Putirka 2009). Therefore, we have dropped unconformities 4 and 5 of Kirkwood Valley from our numbering system, and renumber unconformity 6 of Busby *et al.* (2008a) as unconformity 4 (Figure 2). As is customary, the sequence that overlies an unconformity is assigned the same number as the unconformity (Busby and Putirka 2009).

### *Sequence 1*

Unconformity 1 is mapped as the contact between the undifferentiated Mesozoic granitic rocks (Kgu) or Jurassic–Triassic metamorphic rocks (JTrm), and Tertiary volcanic rocks (Figure 2). Many lines of evidence support the interpretation that this unconformity formed by uplift and unroofing of the Cretaceous batholith during Late Cetaceous to Palaeocene low-angle subduction (see discussion in Busby and Putirka 2009). Palaeorelief on unconformity 1 is measured from the lowest Tertiary unit to the highest preserved granitic basement, and does not account for fill that is higher than granite. Therefore, these numbers represent a minimum amount of relief, as both the granite and the Tertiary fill

have eroded away. In the Kirkwood Valley–Carson Pass map area, the vertical relief on unconformity 1 is up to ~650 m (2100 ft; Busby *et al.* 2008a). In the northern palaeotributary at Horsethief Canyon (Figure 2), the preserved vertical relief on unconformity 1 is 580 m (1900 ft), while in the southern palaeotributary it is 340 m (1100 ft). The base of the palaeocanyon is V-shaped at Horsethief Canyon: the base of the palaeocanyon is less than 60 m (195 ft) wide, but it widens to 250 m (820 ft) at the top of the fluvial sandstone unit (Tvs) and to 1.5 km (~5000 ft) at the top of the fluvial conglomerate and sandstone unit (Tvf1). Elsewhere, the base of the palaeocanyon is highly irregular in shape. For example, on the Sierra crest north of Carson Pass, the palaeocanyon has a very steep wall defined by a Jurassic metamorphic fin (Figure 2(a)), and a less steep wall cut into Cretaceous granitic rock (Figure 3(a)).

Like all palaeocanyons of the central Sierra Nevada (Busby and Putirka 2009), the oldest fill in the Hope Valley–Carson Pass–Kirkwood palaeocanyon consists of Oligocene rhyolitic ignimbrites that were erupted from central Nevada (Faulds *et al.* 2005; Garside *et al.* 2005). The southern palaeotributary was clearly active during the Oligocene, because it contains outcrops of Oligocene ignimbrites south of Markleeville Peak (Figure 9(a)). The northern palaeotributary lacks primary ignimbrite deposits, indicating that it was either inactive during the Oligocene, or all Oligocene rocks were eroded away during the development of unconformity 2; the latter interpretation is supported by the presence of ignimbrite clasts in the basal fluvial sandstone deposits (Tvs).

### *Sequence 2*

Unconformity surface 2 is mapped as an erosional surface between Oligocene ignimbrites below and Miocene andesitic volcaniclastic rocks above (Figure 2). It merges with unconformity 1 where the Valley Springs Formation is not present, such as in the northeastern palaeotributary. In the Kirkwood Valley–Carson Pass area, this unconformity has a maximum vertical relief of 291 m and a lateral extent of 1.5 km. We are unable to accurately measure the depth of unconformity 1 in the Hope Valley area because it is cross-cut by Markleeville Peak intrusions. Throughout the central Sierra Nevada, Oligocene ignimbrites are commonly preserved below unconformity 2 at the base of palaeocanyons or higher on palaeocanyon walls on palaeoledges that were created by joints in the granitic basement rock (Busby *et al.* 2008b). This indicates that the ignimbrite canyon fill was very thick before it was largely eroded away during the development of unconformity 2 (Figure 9(b)). This unconformity may have formed in response to thermal uplift and regional extension at the onset of Ancestral Cascades arc volcanism in what is now the central Sierra Nevada (Busby and Putirka 2009).

In the Hope Valley to Sierran crest area, the basal deposits of sequence 2 consist of volcanic fluvial sandstones (Tvs), which locally pass upwards into stratified cobble breccia–conglomerate deposits of Elephant's Back (Figure 2). The volcanic fluvial sandstone unit (Tvs) is finer grained and better sorted than any other volcaniclastic map unit in the palaeocanyon, and may represent relatively distal deposits from a volcanic source well east of Carson Pass. However, this relatively thin unit is overlain by about 16–14 Ma block-and-ash-flow tuffs, and intrusive activity began in the area while sequence 2 was deposited (intrusions of Little Round Top; Figure 2). Furthermore, the contact between the volcanic fluvial sandstone (Tvs) and the overlying block-and-ash-flow tuff at Jeff Davis Peak (Tphaba) is an erosional unconformity (Figure 2), with 60 m (200 ft) of relief. All of these observations are consistent with the interpretation that unconformity 2 records uplift associated with a thermal pulse as arc volcanism swept westwards into the area.

Unconformity 2 merges with unconformity 1 on the Sierran crest north of Carson Pass. Here, the sequence 1 ignimbrites and the sequence 2 fluvial sandstone unit are absent, and the basal palaeocanyon fill consists of a sequence 2 trachyandesite block-and-ash-flow tuff (Thaba1) dated at 15.01 ± 0.06 Ma (recalculated from Busby *et al.* 2008a; Table 3). This unit passes down-palaeocanyon (westwards) into interstratified debris-flow and fluvial deposits (Figures 2(b) and 9(b)). Several hundred thousand years later, the trachyandesite block-and-ash-flow tuff (Thaba1) was overlain by the 13.61 ± 0.16 Ma andesite block-and-ash-flow tuff (Thaba2).

In summary, sequence 2 volcaniclastic strata and age-correlative intrusions preserve a record of ~16–14 Ma arc magmatism within the area of the palaeocanyon as well as sedimentation of volcanic debris derived from more distal areas to the east.

### *Sequence 3*

Unconformity 3 is mapped as an erosional surface between block-and-ash-flow tuffs and reworked equivalents below, and a thick, widespread fluvial conglomerate and sandstone unit (Tvf1) above. Between the Sierran crest at Carson Pass and Kirkwood Valley, this unconformity has a maximum vertical relief of 315 m (1030 ft), extends across the entire 7–8 km width of the palaeocanyon, and has been traced for 18 km along the length of the palaeocanyon. In the southeastern palaeotributary, this unconformity surface is obscured by the Markleeville Peak intrusion. In the northeastern palaeotributary, unconformity 3 lies at the bottom of a narrow part of the palaeocanyon, so it is very limited in lateral extent. Geochronological and stratigraphic constraints place the cutting of unconformity 3 at between 13.5 and 11 Ma (Figure 9(c)). However, age constraints from other palaeocanyons in the central Sierra show this unconformity formed at 11 Ma, during faulting associated with the inception of the Sierra Nevada microplate (Busby and Putirka 2009).

The fluvial conglomerate sandstone unit (Tvf1) forms a coarsening-upward sequence 370 m (1220 ft) thick along the Sierran crest north of Carson Pass. There, the base of the unit is similar to the fluvial sandstone unit (Tvs; Figure 4(h)), but upsection, the fluvial conglomerate sandstone unit (Tvf1) becomes more conglomeratic, and debris-flow deposits are interbedded with fluvial conglomerates at the top (Tvdf1; Figure 2). Additionally, the sequence 3 fluvial conglomerate and sandstone (Tvf1) passes gradationally upwards into the lower debris-flow deposit (Tvdf1) at Horsethief Canyon. This apparent progradation (Figure 9(c)) may record an up-palaeocanyon (eastwards) increase in volcanic activity.

Our new mapping shows that unconformities 4 and 5 in Kirkwood Valley (Busby *et al.* 2008a) do not extend beyond that small area (Figure 2(b)). Although we correlate the lower volcanic debris-flow deposit (Tvdf1) on the east side of the Hope Valley Graben with the lower volcanic debris-flow deposit (Tvdf1) of Kirkwood Valley, it could also be in part age-correlative with the block-and-ash-flow tuff there (Taba2; Figure 2; Busby *et al.* 2008a).

Volcanic necks forming Pickett and Hawkins Peaks are included in the same sequence as the lower debris-flow deposits (Tvdf1), because these intrusions are of the same age (10.77 ± 0.10 Ma) as peperitic intrusions within the lower debris-flow deposit at Kirkwood Valley (10.72 ± 0.12 Ma; Table 4), which there lie beneath unconformity 4 (unconformity 6 of Busby *et al.* 2008a). The peperitic margins on the intrusion in Kirkwood Valley indicate that the lower debris-flow deposits were water-saturated and unlithified when they were intruded, and are thus penecontemporaneous with the intrusion (Busby *et al.* 2008a). These intra-canyon intrusions passed upwards into lava domes that shed block-and-ash-flows into the canyon (Figure 9(d)).

### *Sequence 4*

As noted above, this is sequence 6 of Busby *et al.* 2008a (Figure 2). Unconformity 4 is mapped as an erosional surface beneath ~ 6 Ma volcanic rocks. In the westernmost part of the palaeocanyon, west of Kirkwood Valley and east of Silver Lake, unconformity 4 cuts through all Tertiary strata to granitic basement below the palaeocanyon, a depth of ~300 m (994 ft; Busby *et al.* 2008a). In Kirkwood Valley, unconformity 4 cuts down 120 m into the lower volcanic debris-flow unit (Tvdf1) of sequence 3, which is there dated at ≥ 10 Ma by peperitic intrusions interpreted to be penecontemporaneous with the debris-flow deposits (Busby *et al.* 2008a; Figure 2). Farther east in the palaeocanyon at the Sierran crest, unconformity 4 cuts into the volcanic fluvial conglomerate and sandstone (Tvf1), also of sequence 3 (Figure 2). The unconformity surface on top of the volcanic fluvial conglomerate and sandstone (Tvf1) has relatively low relief, of about 30 m (100 ft), perhaps because the top of the volcanic fluvial conglomerate and sandstone unit formed a laterally extensive planar surface that was resistant to erosion. Unconformity 4 locally merges with unconformity 3 along the Sierran crest, where intra-canyon palaeoridges composed of sequence 2 block-and-ash-flow tuff units (Thaba1 and Thaba2) are directly overlain by sequence 4 basalt lava flows (Tbl) and debris-flow deposits (Tvdf2). East of the Hope Valley graben, the ~ 6 Ma volcanic rocks that overlie unconformity 4 are replaced by ~ 6 Ma subvolcanic intrusions, whose eruptive equivalents have been eroded away; thus, unconformity surface 4 has also been eroded at the eastern mapped limit of the Hope Valley–Carson Pass–Kirkwood palaeocanyon system (Figure 2).

The oldest dated unit in sequence 4 is the Carson Pass basalt lava flow unit (Tbl) along the Sierran crest north of Carson Pass (Figure 2), dated at 6.95 ± 0.20 Ma (recalculated from Busby *et al.* 2008a; Table 3). The second oldest dated unit in sequence 4 is the hornblende andesite lava flow sequence (Thall and Thalu; Figure 2), dated at 6.22 ± 0.14 Ma (Table 3). Both the basalt lava flow unit and the andesite lava flow units are overlain by the upper volcanic debris-flow deposit (Tvdf2), which occurs as erosional remnants along the Sierran crest as far north as Steven's Peak (Figure 2). This debris-flow unit does not occur in the westernmost mapped part of the palaeocanyon at Kirkwood Valley (Busby *et al.* 2008a; Figure 2); it is not known whether this area was beyond the depositional limit of the unit, or if its absence there indicates the presence of a local erosional unconformity within sequence 4. At Kirkwood Valley, unconformity 4 is overlain by the up to 300 m-thick Sentinels pyroxene block-and-ash-flow tuff (Taba3; Figure 2 of Busby *et al.* 2008a), which was deposited across the width of this segment of the palaeocanyon. The Sentinels pyroxene andesite block-and-ash-flow tuff was dated at 6.18 ± 0.12 Ma (recalculated from Busby *et al.* 2008a; Table 4) and tentatively correlated with the Red Lake Peak pyroxene andesite block-and-ash-flow tuff, on the basis of stratigraphic position, lithology, and mineralogy by Busby *et al.* (2008a). New $^{40}Ar/^{39}Ar$ dates of 6.29 ± 0.10 to 6.13 ± 0.34 Ma on the Red Lake Peak pyroxene andesite block-and-ash-flow tuff (Tpaba; Figure 8(e,f); Table 3) show that these two units are of the same age, supporting this correlation. These ages also constrain the maximum duration of deposition for the upper volcanic debris-flow deposit (Tvdf2) to about 0.8 Ma.

### *Sequence 4 intrusions*

On the map key and correlation diagram of Figure 2(b), intrusions east of the Hope Valley graben in sequence 4 are included even though they are not stratified rocks, because they are the same age as extrusive rocks of sequence 4 (Table 3). The Markleeville Peak intrusive complex (Thbdi) consists of multiple small plugs, including hornblende–biotite

dacite, dated at 6.34 ± 0.14 Ma, hornblende–biotite andesite, dated at 6.18 ± 0.14 Ma, and hornblende basaltic andesite (Figures 5 and 6; Table 2). These $^{40}Ar/^{39}Ar$ ages are younger than but overlap the K/Ar age of 6.9 ± 0.7 Ma reported by Mosier (1991). The intrusive complex and the altered andesite (Taa) are intruded by hornblende andesite dikes and plugs (Thadp) that are dated at 6.37 ± 0.24 Ma, which, within error, are the same age as the rocks they intrude.

### *Sequence 3 or 4 intrusions*

The Horsethief Canyon hornblende–biotite andesite intrusion (Thbai; Table 1) is included in sequence 4 due to the presence of biotite, which is also found in the Markleeville Peak intrusions (Thbdi). It intrudes sequence 3 volcanic debris-flow deposits (Tvdf1), so it could be age equivalent to sequence 3 rather than sequence 4.

The olivine basaltic intrusion (Tbi) at Pickett Peak also is undated. We tentatively include it in sequence 4, because the only other basalt in the area (Tbl at the Sierran crest) erupted during sequence 4.

### *Summary of sequence stratigraphy*

We recognize four major unconformity-bounded units in the Hope Valley–Carson Pass–Kirkwood palaeocanyon system (Figure 9). Unconformity 1 records the unroofing of the Mesozoic Sierra Nevada batholith to mesozonal levels in Late Cretaceous to Palaeocene time. The palaeocanyon was later filled with sequence 1 Oligocene ignimbrites erupted from sources in central Nevada, over a timespan of millions of years (Figure 9(a)). These ignimbrites were largely eroded from the canyon during development of unconformity 2, and overlain by block-and-ash-flow tuffs that record the onset of arc magmatism in the central Sierra Nevada (Figure 9(b)). These were reworked down the palaeocanyon into debris-flow and fluvial deposits (Figure 9(b)). These deposits were in turn eroded during the development of unconformity 3, and overlain by volcanic fluvial deposits of sequence 3 (Figure 9(c)). In most localities, the fluvial deposits that pass gradationally upwards into volcanic debris-flow deposits (Figure 9(d)) are also included in sequence 3, because the erosional surfaces between these units in Kirkwood Valley (unconformities 4 and 5 of Busby *et al.* 2008a) are areally restricted. Peperitic intrusions in the west part of the palaeocanyon at Kirkwood Valley are included in sequence 3, as are volcanic necks of the same age in the northeastern palaeotributary; these presumably formed feeders for andesite lava domes. Unconformity 4 (Figure 9(e)) is the youngest unconformity preserved in the palaeocanyon, and locally cuts down to granitic basement. Sequence 4 has the bulk of the primary volcanic rocks in the palaeocanyon fill, including basaltic and andesitic lava flows, and basaltic andesite to andesite block-and-ash-flow tuffs, as well as their reworked equivalents in the form of volcanic debris-flow deposits, and it lacks fluvial deposits. During deposition of sequence 4 volcanic rocks, the southeastern palaeotributary was intruded by the Markleeville Peak dacite and andesite plugs, which hydrothermally altered their roof rocks (Figure 9(e)). We infer that this relatively large intrusive complex was emplaced within an incipient Hope Valley graben (Figure 9(e)). We also infer that the andesite lava flows erupted after movement on the Red Lake Peak fault began, as they are restricted to the hanging wall of that fault and banked against it. Furthermore, debris-flow deposits that overlie the lava flows on the hanging wall of the fault have megablocks that could represent material that avalanched off the developing

fault. Ultimately, the palaeocanyon was disrupted by the development of the Hope Valley Graben.

## Hope Valley Graben

In this section, we provide new age controls on the development of the range-front fault system at Carson Pass, and provide estimates of the amount of offsets on these faults. We propose a new term, 'Hope Valley Graben', for the structure of the range front at Carson Pass.

The Hope Valley area marks a change in geomorphological style of the Sierra Nevada range front. From the south of Hope Valley, the Sierra Nevada frontal fault system forms a narrow, steep east-facing escarpment (Figure 1(a)). In that segment, steep river canyons run east from the crest to the Owens Valley. In contrast, to the north of Hope Valley, the Sierra Nevada frontal fault system forms the western boundary of the Tahoe Graben, and the northern Sierra Nevada is broken by a series of north–northwest-striking faults (Figure 1(a)). The rivers in the Hope Valley and Tahoe area (West Fork Carson and Upper Truckee Rivers, respectively) run north–south on relatively gentle gradients, in contrast to rivers to the south. The Hope Valley Graben is a much smaller, shallower structure than the Tahoe Graben, but because it is not filled by a lake, it offers a relatively complete view of its structure.

The Hope Valley Graben has historical significance as well. Our new mapping shows that the fault that forms the western boundary of the graben, herein named the Red Lake Fault, takes a major right step or bend under Red Lake (Figure 2(a)). The range front relief is much gentler at this bend or stepover, indicating that it is a lateral ramp. Indeed, the highway over Carson Pass exploited this ramp until 1977, when the modern highway was blasted out of the mountainside north of Red Lake (Figure 2(a)). Even more interestingly, a Forest Service display at the top of what we interpret to be a lateral ramp tells visitors of the fact that the pioneers made use of the relatively gentle relief here to pull their wagons over the pass.

### *Western graben margin: Red Lake Fault*

The Red Lake Fault runs from Upper Blue Lake to Red Lake, and continues north buried under Quaternary deposits in Hope Valley, creating the 600+ m (2000+ ft) escarpment east of the Sierran crest ridge (Figure 2(a)). Armin *et al.* (1984) previously ended this fault below the volcaniclastic rocks on top of Red Lake Peak, where we mapped a metamorphic fin that forms a palaeocanyon wall. Instead, we infer that this fault bends or steps to the right at Red Lake (Figure 2(a)).

Just south of Red Lake, the Red Lake Fault places Cretaceous granite against Miocene volcanic rocks (Figure 3(b)). The fault surface is hidden by 10 m-wide zone of trees and talus along old Highway 88, where the upper andesite lava flow (Thalu) strikes into granitic rock. Beneath the lower lava flow (Thall), the fluvial conglomerate and sandstone unit (Tvf1) crops out along Red Lake's southeastern shore. This fluvial deposit also crops out at Red Lake Peak, so we have used this unit to determine a minimum offset of 365 m (1200 ft) across the Red Lake Fault (Figure 3(a)). This is a minimum, because the base of the fluvial unit on the down-dropped side of the fault is not exposed. However, a check on this estimate is provided by the offset of the stratified cobble breccia-conglomerate (Tsb) along the Red Lake Fault. This unit lies at the base of Elephant's Back on the footwall side of the fault in the southern end of the hills east of the hanging wall. A minimum offset

estimate of ~400 m (1300 ft) is consistent with the estimate for offset of the fluvial conglomerate and sandstone unit (Tvf1 offset 365 m; Figure 3(b)). The andesite lava flows (Thall and Thalu) are restricted to the hanging wall of the Red Lake Fault and abut it directly (Figure 2). This may indicate that the fault served as a conduit for the eruption of the lava flows, or it forms a buttress unconformity with the lava flows.

Farther south along the Red Lake Fault, the altered andesite unit (Taa) is down-dropped against granitic basement (Figure 2). In this area, a 40 m-wide zone of shattered granite is intruded by a porphyritic andesite, labelled as a body of altered andesite (Taa) within the granitic rock (Figure 4(f)). This non-brecciated andesite likely formed due to magma rising along the fault and intruding brecciated granite along the fault zone. This intrusion is propylitically altered and therefore not suitable for Ar/Ar dating. However, the presence of an altered andesite intrusion in shattered granitic rocks along the fault zone indicates that volcanism and faulting overlapped in time, and that the fault started slipping before magmatism ceased. Because most of the volcanic and intrusive activity in the map area occurred at ~6 Ma, and the intrusions within the altered andesite are dated at ~6 Ma (Figure 2), we tentatively interpret that to be the age of the intrusion in the brecciated granite. An up to 750 m (~2500 ft) wide zone of brecciated and sheared granite extends south from the altered andesite intrusion for at least 1500 m (~4900 ft). This zone of deformed granite has numerous calcite veins up to 2 m wide by 30 m long, which trend 340°, the same orientation as the fault (Figure 2(a)).

### *Eastern graben margin: Hope Valley Fault*

The Hope Valley Fault runs through the centre of the map area, along the east side of Hope Valley (Figure 2(a)). It forms a 365 m (1200 ft) tall, west-dipping topographic escarpment in granitic rock on the east side of Hope Valley, suggesting that it is a west-dipping normal fault. Otherwise, it is hidden by Quaternary deposits or cuts altered rocks in which it is difficult to identify.

We propose that the altered andesites at the south end of Hope Valley (unit Taa) are altered roof rocks of the Markleeville Peak intrusions, downfaulted into the Hope Valley Graben. This interpretation is supported by the presence of small, irregularly shaped hornblende–biotite dacite intrusions, unique to the Markleeville Peak intrusive complex in the map area, which cut the altered rocks west of the fault. These are interpreted to be roof rocks of the intrusive complex, which we infer forms a continuous body beneath the altered rocks in the graben. A crude minimum estimate of 370 m (1200 ft) offset along the Hope Valley Fault can be made using the offset between the base of the altered unit on the hanging wall (west of the fault) and the highest point on the eroded top of the intrusion on the footwall (east of the fault; Figure 3(c)), assuming that the top of the intrusion was relatively flat.

### *Possible Horsethief Canyon Fault*

Armin *et al.* (1983) mapped a fault along Horsethief Canyon, between granitic rocks to the west (Kgu) and undivided Tertiary volcaniclastic deposits to the east that we map as units Tvs, Tvf1, and Tvdf1 (Figure 2). We see no evidence for a fault there. There is no topographic escarpment along this proposed fault, nor does it appear to continue south through Tertiary strata of Hawkins Peak and Pickett Peak (Figure 2). The lower volcanic debris-flow deposit unit (Tvdf1) occurs on both sides of Horsethief Canyon, and although the base of this unit rests on granitic basement at a higher elevation west of Horsethief

Canyon than it does on the east side, this is likely a palaeotopographic effect. Thus, the modern Horsethief Canyon follows a steep, 550 m (1800 ft) high palaeocanyon wall. Instead of a fault, we use our more detailed lithofacies mapping to define a palaeocanyon with a V-shaped base that widens upwards (Figure 2).

### *Hope Valley Graben: symmetrical in south and asymmetrical in north*

At the south end of our map area (Figure 2), we estimate subequal normal offset across the Hope Valley Graben between the Red Lake Fault on the east and the Hope Valley Fault on the west (Figure 3). However, the Hope Valley Fault appears to die out to the north (Figure 2), whereas normal offset on the Red Lake Fault appears to increase northwards. The granitic escarpment increases from $<425$ m (1400 ft) near Elephant's Back to 800 m (2600 ft) at Steven's Peak (Figure 2). Along the northern segment of the Red Lake Fault, the base of the palaeocanyon west of the graben lies at an elevation of $\sim 2530$ m (8400 ft), while the base of the palaeocanyon east of the graben at Horsethief Canyon is 430 m (1400 ft) lower. This is consistent with the interpretation that normal offset on the Red Lake Fault grows northwards, while the Hope Valley Fault dies out northwards.

### *Possible role of faults in emplacement of igneous rocks*

We propose that faults of the Hope Valley Graben guided the emplacement of magmas of the Ancestral Cascades arc. Most significant is emplacement of the Markleeville Peak Center (Thbdi) in the south end of the Hope Valley Graben. This $\sim 6$ km diameter centre is one of the largest volcanic centres we have recognized in the central Sierran segment of the Ancestral Cascades arc (Busby and Putirka 2009). Furthermore, it forms part of an extensive alteration zone (altered andesite, Taa) that extends southwards along range-front faults towards Ebbetts Pass (Wilshire 1956, and our unpublished data). This alteration is the effect of hydrothermal activity associated with major $\sim 6$ Ma magmatism and faulting in the area. Also significant is the emplacement of andesite lava flows (Thall and Thalu) and interstratified block-and-ash-flow tuffs (Thaba3) on the graben floor adjacent to the Red Lake Fault. Last, although the source of the $6.95 \pm 0.20$ Ma basalt lava flows is not known, their location just down-palaeocanyon from the Red Lake Fault may indicate that incipient faulting controlled their eruption and emplacement.

### *Lack of evidence for transtension in the Hope Valley Graben*

The GPS velocity field for the central Sierra Nevada has displacements consistent with westward extension and northwest-directed shear (Oldow *et al.* 2001). Earthquake focal plane mechanisms for the area also suggest a present-day right-lateral transtensional stress or strain setting (Oldow 2003; Unruh *et al.* 2003). However, the Hope Valley–Carson Pass palaeocanyon system does not appear to be offset in a strike-slip sense (Figure 1(b)), perhaps indicating that lateral motion is partitioned on faults farther east.

## Conclusions

In the Carson Pass area, Oligocene ignimbrites and Miocene calc-alkaline volcanic and volcaniclastic rocks fill a palaeocanyon that was carved into mesozonal granitic basement between Cretaceous and Eocene time. Miocene volcanic–volcaniclastic and intrusive rocks form part of the Ancestral Cascades arc, and range from mafic to silicic compositions: they include olivine basalts, pyroxene basaltic andesites, hornblende–pyroxene andesites,

and hornblende–biotite dacites, with a minor rhyolitic intrusion. We found no consistent trend in composition versus age for these volcanic rocks, nor did we find a consistent trend in dominant compositions of clasts in fluvial or debris-flow deposits.

Our new $^{40}Ar/^{39}Ar$ age data show that three phases of Miocene volcanism occurred in the Hope Valley–Carson Pass region (Figure 2(b)): at about 16–13.5 Ma (middle Miocene), 11–10 Ma (early late Miocene), and 7–6 Ma (late Miocene). These three pulses in volcanism are recognized across the central and northern Sierra (Busby and Putirka 2009). Volcanic activity in the Hope Valley–Carson Pass area resulted in emplacement of small-volume block-and-ash-flow tuffs and lesser lava flows, which were reworked down-palaeocanyon into volcaniclastic debris-flow and fluvial deposits. Intrusive plugs less than ~250 m (820 ft) in diameter are scattered throughout the area, and may represent feeders to some of the primary volcanic deposits. The Markleeville Peak intrusion (Thbdi) is the largest in the area; its intrusions are exposed across a width of ~3 km and are inferred to lie beneath the altered andesite (Taa) for an additional ~3 km to the west. We infer that late Miocene (7–6 Ma) magmas exploited the Red Lake and Hope Valley faults, which continued to move after this time, and we have found no evidence for faulting in the map area before that time. Thus, while minor middle Miocene and early late Miocene volcanism occurred in the area prior to any recognized fault activity, we propose that major volcanism occurred at the onset of range-front faulting here.

The volcanic and volcaniclastic rocks of Hope Valley are preserved in a palaeocanyon carved into Mesozoic basement rocks. In this paper, we integrated the sequence stratigraphic analysis of the Carson Pass–Kirkwood Valley segment of the palaeocanyon fill, described by Busby *et al.* (2008a), with analysis of a more headward part of the palaeocanyon in the Hope Valley–Carson Pass segment (Figures 2 and 9). In the Hope Valley segment, we identified two palaeotributaries that merge at the present-day Sierran crest to form an over 7 km wide palaeocanyon that was at least 550 m (1800 ft) deep. The southern palaeotributary is 6 km wide and 240 m (800 ft) deep, whereas the northern palaeotributary is up to 10 km wide and over 750 m (2500 ft) deep. Detailed lithofacies mapping of Oligocene through Miocene fill of these palaeocanyons is used to identify four major incision events. The first incision occurred between about 83 and 30 Ma (unconformity 1), and is the contact between Mesozoic basement rocks and Oligocene ignimbrites of sequence 1. The ignimbrites were largely eroded sometime between 23 and 16 Ma (unconformity 2), and the palaeocanyons were filled with volcanic fluvial sandstones and andesitic block-and-ash-flow tuff deposits that pass downstream to volcanic fluvial and debris-flow deposits (sequence 2). Between 13.5 and 11 Ma, the palaeocanyon was reincised (unconformity 3) and then filled with andesitic volcaniclastic debris (sequence 3). Also included in sequence 3 are ~10.7 Ma shallow-level intrusions at Pickett Peak and Hawkins Peak (Figure 2(a)) that were emplaced coevally with a peperitic andesite dike at Kirkwood Valley (Figure 2(b)). Sometime between the emplacement of the 10.7 Ma volcanic intrusions and renewed volcanic activity at ~7 Ma, the canyon was reincised (unconformity 4; Figure 2(b)). Regional stratigraphic relations indicate that this happened at about 8 Ma (Busby and Putirka 2009). From 7 to 6 Ma (sequence 4), the region was rife with volcanic and intrusive activity (sequence 4). We propose that the Red Lake and Hope Valley faults began moving at this time, but slip could have commenced any time after 10 Ma.

Hope Valley is a full graben bounded on the west by the Red Lake Fault and on the east by the Hope Valley Fault. The Red Lake Fault has at least 400 m (1300 ft) of normal offset since its initiation. The Hope Valley Fault has at least 370 m (1200 ft) of normal offset since 6.34 Ma. Both of these faults display subequal offset at the south end of the Hope

Valley Graben, but the Hope Valley Fault dies out to the north, whereas offset on the Red Lake Fault grows by the same amount. The timing of the end of movement along the faults is poorly constrained, because we have found neither volcanic rocks younger than 6 Ma nor scarps in Quaternary deposits.

Recent studies use geodetic and fault focal mechanism data to infer that at least some Sierra Nevada range-front faults have a strike-slip component, i.e. they are transtensional. However, we see no evidence for strike-slip offset of the Hope Valley–Carson Pass–Kirkwood palaeocanyon across the Hope Valley or Red Lake Fault, nor do we see evidence for a fault taking up pure strike-slip motion in the map area.

## Acknowledgements

This work was supported by NSF grant EAR-0711181 (to Busby), NSF grant EAR-0711276 (to Busby and Putirka), and USGS EDMAP grants 05HQAG0010 (to Busby) and 06HQAG061 (to Busby), and a GSA graduate student research grant (to Hagan). We would like to thank our field assistants, including Dana Vukajlovich, Liz Lovelock, Adrian Almanza, Megan Gambs, Chip Hagan, and Senator Kay Hagan. We thank Joyce at the Hope Valley Cafe, for storing gear and providing delicious pie. We thank Steve DeOreo for helping to introduce Hagan to the region, and Duane DeVecchio for visiting the field area and giving geologic advice. Thanks also to Marlon Jean in Putirka's laboratory at CSU Fresno, and Abed Jaouni at the Berkeley Geochronology Center for assistance in the laboratory.

## References

Armin, R.A., John, D.A., and Dohrenwend, J.C., 1983, Geologic map of the Freel Peak 15-minute quadrangle, California and Nevada, Miscellaneous Investigations Series–U.S. Geological Survey, Report: I-1424, scale 1:62,500.

Armin, R.A., John, D.A., Moore, W.J., and Dohrenwend, J.C., 1984, Geologic map of the Markleeville 15 minute quadrangle, Alpine County, California, Miscellaneous Investigations Series–U.S. Geological Survey, Report: I-1474, Scale 1:62,500.

Atwater, T., and Stock, J., 1998, Pacific–North America Plate Tectonics of the Neogene Southwestern United States–An update: International Geological Review, v. 40, p. 375–402.

Bateman, P.C., and Wahrhaftig, C., 1966, Geology of the Sierra Nevada, *in* Bailey, E.H., ed., Geology of northern California: California Division of Mines Bulletin, v. 190, p. 107–172.

Busby, C.J., and Putirka, K., 2009, Miocene evolution of the western edge of the Nevadaplano in the central and northern Sierra Nevada: palaeocanyons, magmatism, and structure: International Geology Review, v. 51, p. 670–701.

Busby, C.J., DeOreo, S.B., Skilling, I., Hagan, J.C., and Gans, P.B., 2008a, Carson Pass–Kirkwood paleocanyon system: Implications for the Tertiary evolution of the Sierra Nevada, California: Geological Society of America Bulletin, v. 120, p. 274–299.

Busby, C.J., Hagan, J.C., Putirka, K., Pluhar, C.J., Gans, P.B., Wagner, D.L., Rood, D.H., DeOreo, S.B., and Skilling, I., 2008b, The ancestral Cascades arc: Cenozoic evolution of the central Sierra Nevada (California) and the birth of the new plate boundary, *in* Wright, J.E., and Shervais, J.W., eds., Ophiolites, Arcs, and Botholiths: A Tribute to Cliff Hopson: Geological Society of America Special Paper 438, p. 331–378.

Camus, G., Gourgaud, A., Moussand-Berthommier, P.-C., and Vincent, P.-M., 2000, Merapi (Central Java, Indonesia): an outline of the structural and magmatological evolution, with a special emphasis to the major pyroclastic events: Journal of Volcanology and Geothermal Research, v. 100, p.139–163.

Chase, C.G., Gregory, K.M., Parrish, J.R., and DeCelles, P.G., 1998, Topographic history of the western Cordilleran of North America and the etiology of climate, *in* Crowley, T.J., and Burke, K., eds., Tectonic boundary conditions for climate reconstructions: Oxford Monographs on Geology and Geophysics, v. 39, p. 73–99.

Clynne, M.A., 1990, Stratigraphic, lithologic and major element geochemical constraints on magmatic evolution at Lassen volcanic center, California: Journal of Geophysical Research, v. 95, p. 19651–19669.

Coney, P.J., and Harms, T.A., 1984, Cordilleran metamorphic core complexes: Cenozoic extensional relics of Mesozoic compression: Geology, v. 12, p. 550–554.

Cousens, B., Prytulak, J., Henry, C.D., Alcazar, A., and Brownrigg, T., 2008, Geology, geochronology, and geochemistry of the Miocene–Pliocene Ancestral Cascades arc, northern Sierra Nevada, California and Nevada: The roles of the upper mantle, subducting slab, and the Sierra Nevada lithosphere: Geosphere, v. 4, p. 829–853.

Curtis, G.H., 1951, The Geology of the Topaz Lake Quadrangle and the Eastern Half of the Ebbetts Pass Quadrangle. 1:125,000 [Unpublished Ph.D. thesis], University of Caliornia, Berkeley.

Curtis, G.H., 1954, Mode of origin of pyroclastic debris in the Mehrten Formation of the Sierra Nevada: University of California Publications in Geological Sciences, v. 29, p. 453–502.

Davis, D.A., Henry, C.D., Garside, L.J., Faulds, J.E., and Goldstrand, P.M., 2000, Eocene–Oligocene paleovalleys cross the Sierra Nevada–Basin and Range boundary, western Nevada and eastern California: Geological Society of America, 2000 annual meeting Abstracts with Programs, v. 32, p. 167.

DeCelles, P.G., 2004, Late Jurassic to Eocene evolution of the Cordilleran thrust belt and foreland basin system, western USA: American Journal of Science, v. 304, p. 105–168.

Dickinson, W.R., 2006, Geotectonic evolution of hte Great Basin: Geosphere, v. 2, p. 353–368.

Dilles, J.H., and Gans, P.B., 1995, The chronology of Cenozoic volcanism and deformation in the Yerington area, western Basin and Range and Walker Lane: Geological Society of America Bulletin, v. 107, p. 474–486.

Dixon, T.H., Robaudo, S., Lee, J., and Reheis, M.C., 1995, Constraints on present-day Basin and Range deformation from space geodesy: Tectonics, v. 14, p. 755–772.

Dixon, T.H., Miller, M., Farina, F., Wang, H., and Johnson, D., 2000, Present-day motion of the Sierra Nevada block and some tectonic implications for the Basin and Range province, North American Cordillera: Tectonics, v. 19, p. 1–24.

Faulds, J.E., Henry, C.D., and Hinz, N.H., 2005, Kinematics of the northern Walker Lane; an incipient transform fault along the Pacific–North American Plate boundary: Geology (Boulder), v. 33, p. 505–508.

Fisher, R.V., and Heiken, G., 1982, Mt. Pelee, Martinique: May 8 and 20, 1902, pyroclastic flows and surges: Journal of Volcanology and Geothermal Research, v. 13, p. 339–371.

Fisher, R.V., and Schminke, H.U., 1984, Pyroclastic Rocks: Berlin, Springer Verlag, 472 p.

Freundt, A., Wilson, C.J.N., and Carey, S., 2000, Ignimbrites and block-and-ash flow deposits, *in* Sigurdson, H., Houghton, B.F., McNutt, S.R., Rymer, H., and Stix, J., eds., Encyclopedia of volcanoes: San Diego, Academic Press, p. 581–599.

Garrison, N., Busby, C., Gans, P.B., Putirka, K., and Wagner, D.L., 2008, A mantle plume beneath California? The Mid-Miocene Lovejoy flood basalt, *in* Wright, J.E., and Shervais, J.W., eds., Ophiolites, Arcs, and Batholiths: A Tribute to Cliff Hopson: Geological Society of America Special Paper 438, p. 551–572.

Garside, L.J., Henry, C.D., Faulds, J.E., and Hinz, N.H., 2005, The upper reaches of the Sierra Nevada auriferous gold channels, *in* Rhoden, H.N., Steininger, R.C., and Vikre, P.G., eds., Geological Society of Nevada Symposium 2005: Reno, Nevada: Window to the World, p. 209–235.

Gradstein, F.M., Ogg, J.G., and Smith, A.G., eds. 2004, A geologic time scale 2004: Cambridge, UK, Cambridge University Press, 589 p.

Hearn, E.H., and Humphreys, E.D., 1998, Kinematics of the southern Walker Lane Belt and motion of the Sierra Nevada block, California: Journal of Geophysical Research, v. 103(B11), 27,033–27,049.

Heiken, G., and Wohletz, K., 1985, Volcanic Ash: Berkeley, CA, University of California Press, 246 p.

Henry, C.D., 2008, Ash-flow tuffs and paleovalleys in northeastern Nevada: Implications for Eocene paleogeography and extension in the Sevier hinterland, northern Great Basin: Geosphere, v. 4, p. 1–35.

Henry, C.D., and Perkins, M.E., 2001, Sierra Nevada–Basin and Range transition near Reno, Nevada: Two-stage development at 12 and 3 Ma: Geology, v. 29, p. 719–722.

Henry, C.D., Faulds, J.E., Garside, L.J., and Hinz, N.H., 2003, Tectonic implications of ash-flow tuffs in paleovalleys in the Western US: Abstracts with Programs: Geological Society of America, v. 35, p. 346.

Hinz, N.H., Faulds, J.E., and Henry, C.D., 2003, Dextral displacement on the Honey Lake fault zone, northern Walker Lane, northeast California and westernmost Nevada; preliminary constraints inferred from Oligocene ash-flow tuff stratigraphy: Geological Society of America, 2003 annual meeting Abstracts with Programs, v. 35, p. 347.

Huber, N.K., 1990, The late Cenozoic evolution of the Tuolumne River, central Sierra Nevada, California: Geological Society of America Bulletin, v. 102, p. 102–115.

Kuiper, K.F., Deino, A.L., Krijgsman, W., Renne, P.R., and Wijbrans, J.R., 2008, Synchronizing the rock clocks of Earth history: Science, v. 320, p. 500–504.

Le Bas, M.J., Le Maitre, R.W., Streckeisen, A., and Zanettin, B., 1986, A chemical classification of volcanic rocks based on the total alkali–silica diagram: Journal of Petrology, v. 27, p. 745–750.

Lindgren, W., 1911, The Tertiary Gravels of the Sierra Nevada of California: Washington, DC, United States Geological Survey, 222 p.

Miyabuchi, Y., 1999, Deposits associated with the 1990–1995 eruption of Unzen volcano, Japan: Journal of Volcanology and Geothermal Research, v. 89, p. 139–158.

Morton, J.L., Silberman, M.L., Bonham, H.F., Garside, L.J., and Noble, D.C., 1977, K-Ar ages of volcanic rocks, plutonic rocks, and ore deposits in Nevada and estern California–Determinations run under the USGS-NBMG cooperative program: Isochron/West, v. 20, p. 19–29.

Mosier, D.L., 1991, Tertiary Volcanic History of the Markleeville Peak Area, Alpine County, California [MS thesis]: California State University, Hayward.

Oldow, J.S., 2003, Active transtensional boundary zone between the western Great Basin and Sierra Nevada block, western U.S. Cordillera: Geology, v. 31, p. 1033–1036.

Oldow, J.S., Aiken, C.L.V., Hare, J.L., Ferguson, J.F., and Hardyman, R.F., 2001, Active displacement transfer and differential block motion within the central Walker Lane, western Great Basin: Geology, v. 29, p. 19–22.

Piper, A.M., Gale, H.S., Thomas, H.E., and Robinson, T.W., 1939, Geology and ground water hydrology of the Mokelumne area, California: United States Geological Survey Water Supply Paper, v. 780, p. 230.

Putirka, K., and Busby, C.J., 2007, The tectonic significance of high-$K_2O$ volcanism in the Sierra Nevada, California: Geology, v. 35, p. 923–926.

Renne, P.R., Swisher, C.C., Deino, A.L., Karner, D.B., Owens, T., and DePaolo, D.J., 1998, Intercalibration of standards. Absolute ages and uncertainties in $^{40}Ar/^{39}Ar$ dating: Chemical Geology (Isotope Geoscience Section), v. 145, p. 117–152.

Saucedo, G.J., and Wagner, D.L., 1992, Geologic map of the Chico Quadrangle, California, 1:250,000, Regional Geologic Map Series No. 7A: Sacramento, CA: California Division of Mines and Geology.

Schweickert, R.A., Lahren, M.M., Smith, K.D., Howle, J.F., and Ichinose, G., 2004, Transtensional deformation in the Lake Tahoe region, California and Nevada, USA: Tectonophysics, v. 392, p. 303–323.

Slemmons, D.B., 1966, Cenozoic volcanism of the central Sierra Nevada, California, Geology of Northern California: Bulletin of the California Division of Mines and Geology, v. 170, p. 199–208.

Stockli, D.F., Surpless, B.E., Dumitru, T.A., and Farley, K.A., 2002, Thermochronological constraints on the timing and magnitude of Miocene and Pliocene extension in the central Wassuk Range, western Nevada: Tectonics, v. 21, p. 1028.

Surpless, B.E., Stockli, D.F., Dumitru, T.A., and Miller, E.L., 2002, Two-phase westward encroachment of Basin and Range extension into the northern Sierra Nevada: Tectonics, v. 21, p. 1002.

Thatcher, W., Foulger, G.R., Julian, B.R., Svarc, J.L., Quily, E., and Bawden, G.W., 1999, Present-day deformation across the Basin and Range Province, Western United States: Science, v. 283, p. 1714–1718.

Trexler, J.H., Jr, Cashman, P.H., Muntean, T., Schwartz, K., Ten Brink, A., Faulds, J.E., Perkins, M., and Kelly, T., 2000, Neogene basins in western Nevada document the tectonic history of the Sierra Nevada-Basin and Range transition zone for the last 12 Ma, *in* Lageson, D.R., Peters, S.G., and Lahren, M.M., eds., GSA Field Guide: Great Basin and Sierra Nevada, v. 2, p. 97–116.

Unruh, J.R., Humphrey, J., and Barron, A., 2003, Transtensional model for the Sierra Nevada frontal fault system, eastern California: Geology, v. 31, p. 327–330.

Verdel, C., Wernicke, B.P., Ramezani, J., Hassanzadeh, J., Renne, P.R., and Spell, T.L., 2007, Geology and thermochronology of Tertiary Cordillera-style metamorphic core complexes in the Saghand region of central Iran: Geological Society of America Bulletin, v. 119, p. 961–977.

Voight, B., Constantine, E.K., Siswowidjoyo, S., and Torley, R., 2000, Historical eruptions of Merapi Volcano, Central Java, Indonesia, 1768–1998: Journal of Volcanology and Geothermal Research, v. 100, p. 69–138.

Wagner, D.L., and Saucedo, G.J., 1990, Age and stratigraphic relationships of Miocene Volcanic Rocks along the eastern margin of the Sacramento Valley, California, *in* Ingersoll, R.V., and Nilsen, T.H., eds., Sacramento Valley Symposium Guidebook: Pacific Section S.E.P.M., v. 65, p. 143–151.

Wagner, D.L., Saucedo, G.J., and Grose, T.L.T., 2000, Tertiary Volcanic Rocks of the Blairsden Area, Northern Sierra Nevada, California, *in* Brooks, E.R., and Dida, L.T., eds., Field Guide–Geology and Tectonics of the Northern Sierra Nevada; National Association of Geoscience Teachers Far-Western Section Fall Conference–2000: California Division of Mines and Geology Special Publication, v. 122, p. 155–172.

Wakabayashi, J., and Sawyer, T.L., 2001, Stream incision, tectonics, uplift, and evolution of topography of the Sierra Nevada, California: The Journal of Geology, v. 109, p. 539–562.

Wernicke, B.P., 1992, Cenozoic extensional tectonics of the US Cordillera, *in* Burchfiel, B.C., Lipman, P.W., and Zoback, M.L., eds., The Geology of North America, the Cordilleran region: Geological Society of America, Decade in North American Geology Series, v. G-3, p. 553–581.

Wernicke, B.P., Friedrich, A.M., Niemi, N.A., Bennett, R.A., and Davis, D.A., 2000, Dynamics of Plate Boundary Fault Systems from Basin and Range Geodetic Network (BARGEN) and geologic data: GSA Today, v. 10, p. 1–3.

Wilshire, H.G., 1956, The history of tertiary volcanism near Ebbets Pass, Alpine County, California [PhD thesis]: Berkeley, University of California.

Wolfe, J.A., Forest, C.E., and Molnar, P., 1998, Paleobotanical evidence of Eocene and Oligocene paleoaltitudes in midlatitude western North America: Geological Society of America Bulletin, v. 110, p. 664–678.